Investigations of the role of nonlinear couplings in structure formation and transport regulation:

experiment, simulation, and theory

Investigations of the role of nonlinear couplings in structure formation and transport regulation: experiment, simulation, and theory

C. Holland[1]**, P.H. Diamond**[1]**, S. Champeaux**[1,a]**, E. Kim**[1]**,
O. Gurcan**[1]**, M.N. Rosenbluth**[1]**, G.R. Tynan**[2]**, N. Crocker**[2]**,
W. Nevins**[3] **and J. Candy**[4]

[1] Department of Physics, University of California, San Diego, La Jolla, CA 92093, USA

[2] Department of Mechanical and Aerospace Engineering, University of California,
San Diego, La Jolla, CA 92093, USA

[3] Lawrence Livermore National Laboratory, PO Box 808, L-637, Livermore, CA 94551, USA

[4] General Atomics, PO Box 85608, San Diego, CA 92186-5608, USA

Abstract
In this paper, we report on an integrated program of experimental, computational, and theoretical studies of sheared zonal flows and radially extended convective cells, with the aim of assessing the results of theory–experiment and theory–simulation comparisons. In particular, simulations are used as test beds for verifying analytical predictions (specifically locality and directionality of energy transfer) of nonlinear dynamics and to investigate the suitability of bispectral analysis for studying nonlinear couplings. Initial comparisons to experimental results are presented, and future experimental studies are motivated. We also present analytic and numerical work investigating the role of structures in transport.

PACS numbers: 52.35.Ra

1. Introduction

A central challenge of plasma turbulence research in the last decade has been to develop a cohesive picture for understanding how zonal flows [1–3] are generated and regulate [2, 4–8] turbulence. The picture that has emerged (at least for turbulence in the core of tokamaks) is one in which the energy and momentum of turbulent fluctuations is transferred to a slowly varying shear flow (the zonal flow) via the Reynolds stress [9], with the zonal flow in turn shearing or radially decorrelating the turbulence [10, 11]. More recent work has begun the process of understanding the saturation mechanisms of zonal flows. It is also known that the turbulent flux is highly intermittent or 'bursty'. The largest bursts have been suggested to be due to large, radially extended convective cells (often termed 'streamers' [3, 12, 13]) which can be generated by nonlinear couplings and secondary instability processes. It is clear that the role of nonlinear couplings in generating secondary structures

which can greatly affect the turbulence and its associated transport (either to regulate or enhance it) must be thoroughly understood if quantitative predictions for turbulent transport are to be made. Significant strides have been made in both the analytic theory of transport regulation (and enhancement) and computational investigations of turbulent transport, as well as experimental studies of such transport. These advances allow more comprehensive integrated studies of transport to be undertaken, which are necessary if a true predictive capability for turbulent transport is to be developed.

Many of the qualitative predictions (such as shear flow decorrelation of turbulence and the corresponding reduction of transport) from theory have been verified and well documented in experiment and simulation. The aim of this paper is to build upon these previous investigations via the use of more detailed and advanced methods of quantifying the results of simulations and physical experiments. In particular, three issues are addressed in detail:

(1) Quantifying the impact of shear flows on the pathway for nonlinear energy transfer in different models of drift-wave turbulence, such as changes in the directionality, locality, and isotropy of the transfer.

[a] Present address: CEA/DIF, Départment de Physique Théorique Appliquée, B.P. 12, 91680 Bruyéres-le-Chatel, France.

(2) The utility of, and results from, bicoherence studies (and bispectral analysis, in general) as an experimentally realizable tool for quantitative studies of the nonlinear generation and dynamics of shear flows and their impact on turbulence.

(3) The significance and utility of probability distribution function (PDF) based representations of turbulent fluxes, as opposed to local turbulent diffusivities.

For each issue, we seek to compare results from simulation and experiment with expectations from analytic theory. By doing this, we hope to create points of contact between all three approaches to investigations of turbulence upon which future studies can build.

2. Theory overview

The theory of zonal flow generation and their role in regulating turbulence is now well developed. An overview of the existing theory is given here to serve as a guide for the investigations presented in the following sections. In particular, there are several fundamental themes of the theory, which having been examined qualitatively, should now be investigated more thoroughly.

Zonal flows are poloidally and toroidally symmetric ($k_\theta = k_\phi = 0$, finite k_r) shear flows, which are predicted to be generated via radial gradients of the turbulent Reynolds stress

$$\langle \tilde{v}_r \tilde{v}_\theta \rangle \approx \left(\frac{c^2}{B^2} \right) \langle \tilde{E}_r \tilde{E}_\theta \rangle.$$

Such generation can take the form of a parametric instability [14] (which provides an accurate description for initial zonal flow generation via instability of the fastest growing mode), or by a modulational instability [2] of a wide spectrum of drift-waves [15] (related to generation and sustainment of zonal flows in the nonlinearly saturated state). Both the parametric and modulational instability descriptions build upon a presumed scale separation between the drift-wave turbulence and the zonal flows; in particular, two drift-waves of approximately the same wavenumber beat against each other to drive a zonal flow (generally assumed to have $k_r^{ZF} \ll k_r^{DW}$). This assumption implies that the wavevectors of the interacting triad $\langle \phi_{ZF} \tilde{E}_r \tilde{E}_\theta \rangle$ form 'narrow' triangles such as those shown in figure 1, rather than the equilateral triangles expected in traditional fluid turbulence theories for isotropic systems [16] (where $|\vec{k}_1| \approx |\vec{k}_2| \approx |\vec{k}_3|$). Thus, in the modulational instability model, zonal flow generation represents an inverse transfer of kinetic energy (to $|\vec{k}_{ZF}| < |\vec{k}_{DW}|$), similar to what is expected for two-dimensional neutral fluid turbulence [17], but this transfer is nonlocal ($|\vec{k}_{ZF}| \ll |\vec{k}_{DW}|$) and anisotropic (as zonal flows have only finite k_r) in nature, contrary to simple expectations for inverse cascade dynamics in two-dimensional neutral fluids. Quantitative computational and experimental tests of directionality (inverse transfer of kinetic energy), locality (scale separation between drift-waves and zonal flows), and anisotropy would provide useful knowledge of the validity and limitations of this theory. Finally, zonal flows saturate either through weak collisional damping ($\propto \nu_{ii}$) [18] or possibly through nonlinear mechanisms [19–23]; the competition between these various saturation mechanisms represents a current challenge for zonal flow theory.
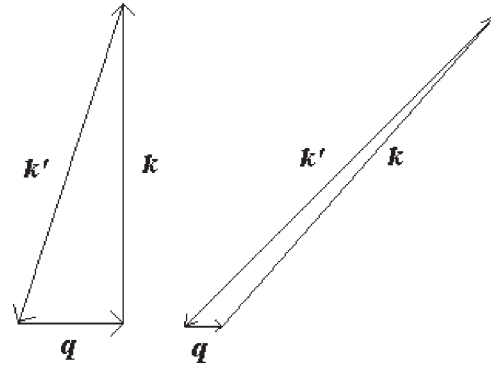
Figure 1. Schematics of zonal flow–drift-wave interactions for zonal flow of wavevector q and two drift-waves of wavevectors k and k'.

There are several different ways for understanding how shear flows are believed to regulate turbulence and the associated transport. On the simplest level, turbulence regulation can be understood by noting that a 'sufficiently strong' shear flow radially decorrelates the turbulence, thereby reducing the effective 'step size' Δr in the turbulent diffusivity $D_{turb} \approx \Delta r^2 / \tau_{corr}$ [10]. One can also view the problem from an energetic standpoint, and note that the sum of zonal flow generation by turbulence and the back-reaction of the zonal flows on the turbulence must conserve total energy (and momentum) [3, 24]. In such an approach, the back-reaction of the zonal flows on the turbulence can be modelled as a quasi-linear diffusion in k_r of an appropriate wave-action variable [25]. The simplest description for such a model is of the form [2]:

$$\frac{\partial \langle N \rangle}{\partial t} - \frac{\partial}{\partial k_r} D \frac{\partial \langle N \rangle}{\partial k_r} = \gamma_{lin}(\vec{k}) \langle N \rangle - \Delta \omega(\vec{k}) \langle N \rangle^2,$$

$$\frac{\partial U}{\partial t} + \nu_{RH} U = \gamma_{RS} U + [\text{noise}], \quad (1)$$

$$U = \sum_q |\phi_q|^2, \qquad D \propto \sum_q q^4 k_\theta^2 |\phi_q|^2.$$

Here, $\langle N \rangle$ is the wave-action density ($= (1 + k_\perp^2)^2 \langle \tilde{\phi}_k \tilde{\phi}_{-k+q} \rangle$ for drift-wave turbulence in the presence of zonal flows [25]), $|\phi_q|^2$ is the zonal flow spectrum, U is defined as the total zonal flow intensity, γ_{RS} the Reynolds stress drive of the zonal flow (which is a nonlinear function of the wave-action and its derivatives, e.g. for the modulational instability,

$$\gamma_{RS} = \gamma_{RS} \left(\frac{\partial \langle N \rangle}{\partial k_r} \right)$$

[2], see equation (3)), and ν_{RH} represents Rosenbluth–Hinton collisional damping [18]. Thus, the radial decorrelation of turbulence is simply diffusion in k_r of wave-action (i.e. the broadening of the turbulent spectrum in k_r appears as a reduced radial correlation length in physical space), and shear suppression simply the transfer of energy from unstable modes that drive transport to stable shear flows which do not. The interested reader is referred to a more complete discussion of this topic in [24].

It should also be noted that the model presented in equation (1) indicates that there is a clear relation between the turbulent diffusivity and the zonal flow saturation mechanisms (here taken to be Rosenbluth–Hinton collisional damping).

This can be seen by noting that in a statistical steady state, $\gamma_{RS} = \nu_{RH}$. Since $\gamma_{RS} \propto \langle N \rangle$, one finds that the turbulent intensity ($\propto \langle N \rangle$ as well) scales with ν_{RH}. And since the turbulent diffusivity χ^{turb} is linearly proportional to the turbulent intensity, one finds $\chi^{turb} \propto \nu_{RH}$. This effect is clearly demonstrated in the work of Lin and co-workers [8].

One can then ask how this regulation of turbulence could be verified in detail by simulations or experiment. Previous investigations have focused on examining changes in radial correlation lengths, as well as quantifying what a 'sufficiently strong' zonal flow spectrum is numerically (generally in terms of the ratio of shearing rate to linear growth rate (in the absence of shear) [26, 27]). Here, we seek to verify some nonlinear aspects of the models. In particular, it is usually found that the magnitude of the zonal flows is much larger than that of the turbulence; see appendix for a discussion of the physics, which sets this ratio. This result follows for two reasons. First, zonal flows have $k_\theta = 0$, and thus cannot couple energy to drift-waves except by some type of Kelvin–Helmholtz or other nonlinear process. Certainly, the standard Kelvin–Helmholtz mechanism is weakened by the sheared magnetic field. However, microscale Kelvin–Helmholtz variants triggered by drift-wave noise may also be possible (see section 3.2 for a more complete discussion of such variants). Second, on account of their symmetry, zonal flows may be thought of as fluctuations of minimal inertia and minimal damping, which favours strong flows. If the dominant nonlinearites governing the drift-wave dynamics are then taken to be convection of internal and kinetic energy by zonal flows (as opposed to like-scale 'eddy–eddy' interactions), examination of the wavevector sum rule $\vec{k}_1^{DW} + \vec{k}_2^{DW} + \vec{k}^{ZF} = 0$ shows that the dominant energy transfer must involve turbulent modes with wavevectors $\vec{k} = (k_r, k_\theta)$ and $\vec{k}' = -(k_r + k_r^{ZF}, k_\theta)$. Thus, a specific signature of shear flow–turbulence interactions (even more specifically, radial decorrelation of turbulent eddies) should be a 'scattering' of energy from some wavevector $\vec{k}$ to other values of k_r at the same k_θ (again reflecting the idea that zonal flows lead to a diffusion of energy in k_r). Conversely, the signature of Reynolds stress driving of the zonal flow will be a transfer of kinetic energy from the drift-waves into the zonal flows. A study of these signatures in various computational models of drift-wave turbulence (both to verify their existence, and quantify their magnitude), along with investigations of the overall directionality, locality and anisotropy of energy transfer, is one of the primary goals of this paper.

3. Shear flows and energy transfer

As described above, an understanding of the impact of zonal flows on nonlinear energy transfer in plasma turbulence is crucial for a detailed understanding of turbulence and transport regulation. Towards this end, an extensive study of shear flow effects on energy transfer in models of drift-wave turbulence has been undertaken. The first step of this study was to analyse the effects of shear flows on energy transfer in simulations of two variants of a basic fluid model for electrostatic curvature-driven drift-wave turbulence. One variant describes toroidal (curvature-driven) ion-temperature gradient (ITG) turbulence (which is generally accepted to be the dominant

source of anomalous particle and ion thermal transport in the core of magnetic confinement devices) [28], while the other describes toroidal electron-temperature gradient (ETG) turbulence (a potential mechanism for anomalous core electron thermal transport) [29]. For the sake of brevity, only a brief summary of the model equations is presented here; the interested reader is referred to the appropriate reference for more complete descriptions and characterizations of the models. The model equations for both instabilities are [28,29]:

$$(\delta - \nabla_\perp^2)\frac{\partial \phi}{\partial t} + \frac{\partial \phi}{\partial y} - \varepsilon \frac{\partial p}{\partial y} - \nu(\nabla_\perp^2)\phi = -\{\phi, \nabla_\perp^2 \phi\},$$
$$\frac{\partial p}{\partial t} + (1 + \eta)\frac{\partial \phi}{\partial y} + \chi \nabla_\perp^4 p = -\{\phi, p\}.$$
(2)

The variables $\phi = (L_n/\rho)|e|\tilde{\phi}/T_e$ and $p = (L_n/\rho)\tilde{p}/p_0$ are the (density mixing length) normalized electrostatic potential and pressure fluctuations, respectively, $\varepsilon = L_n/L_B$, and $\eta = L_n/L_T$; $L_f = -d \ln f_0/dx$. The spatial coordinates x and y are normalized to ρ, and t to L_n/u; the Poisson brackets (right-hand sides) represent electrostatic convection of vorticity $\nabla_\perp^2 \phi$ and pressure fluctuations ($\vec{v}_{E \times B} \cdot \vec{\nabla} f = -\vec{\nabla}\phi \times \hat{z} \cdot \vec{\nabla} f = \hat{z} \cdot (\vec{\nabla}\phi \times \vec{\nabla} f) = \{\phi, f\}$). For the ETG case,

$$\rho = \rho_e = \frac{v_{Te}}{\Omega_{ce}}, \qquad u = v_{Te} = \sqrt{\frac{T_e}{m_e}}$$

and it is assumed that $T_e/T_i = 1$. For the ITG case,

$$\rho = \rho_s = \frac{c_s}{\Omega_{ci}} \qquad \text{and} \qquad u = c_s = \sqrt{\frac{T_e}{m_i}}.$$

Hyperviscosity ($\nu\nabla_\perp^6$) and hyperdiffusion ($\chi\nabla_\perp^4$) are used for finite k_y modes (see later for the treatment of damping of $k_y = 0$ modes).

The key difference between the instabilities lies in the density response to the flux-surface averaged potential [15], which is known to have a strong impact on zonal flow formation. In particular, simulations of ITG turbulence saturate rapidly through zonal flow formation [4–7], while the (toroidal) ETG turbulence simulations show little evidence of zonal flow formation, and saturate much more slowly, at a much higher energy relative to mixing-length levels, via some other nonlinear process [29, 30]. It should be noted that formation and role of zonal flows (and zonal magnetic fields [31, 32]) in ETG turbulence is still an area of current research; in particular, recent work [33] has demonstrated that ETG zonal flows will be collisionally damped (proportional to a combination of ν_{ee} and ν_{ei}), in a completely analogous manner to the Rosenbluth–Hinton mechanism for ITG-driven zonal flow damping (i.e. ITG zonal flows damp on trapped ions, ETG zonal flows damp on trapped electrons (and ions)). Nevertheless, the formation of zonal modes in more complex ETG models is still certainly a possibility, and has been observed in simulations of slab ETG turbulence [34]. However, the simple model used here does not seem to exhibit their formation. The quantity $\delta = \delta(k_y)$ is a simple attempt to include the response of density perturbations to the flux-surface averaged potential (represented here as an average over y). For all finite values of k_y, $\delta(k_y) = 1$. If $\delta(0) = 0$, the above equations describe ITG-like turbulence, while if $\delta(0) = 1$, they describe ETG-like turbulence (under the additional transform $y \to -y$). In the language of [2, 31],

one could write the effective zonal flow growth rate from modulational instability as:

$$\gamma_q^{\mathrm{ZF}} = \frac{q^4 \rho^4}{\delta(0) + q^2 \rho^2} \int \mathrm{d}^2 k \, \frac{k_y^2}{\Lambda_k} R(k, q) \left(-k_r \frac{\partial \langle N \rangle}{\partial k_r} \right). \quad (3)$$

Here, q is the wavenumber of the zonal flow, $R(k, q)$ is a group-phase resonance function (defined as $R(k, q) = 1/(\gamma_k - \mathrm{i}(\Omega_q - \vec{q} \cdot \vec{v}_g))$, where Ω_q is the zonal flow frequency ($\cong 0$), and $\vec{v}_g = \partial \omega_k / \partial \vec{k}$ is the group velocity of the turbulent fluctuations with wavenumber $\vec{k}$), and $\Lambda_k = N_k / \langle |\tilde{\phi}_k \tilde{\phi}_{-k+q}| \rangle$. Thus, one could say that zonal flows have different 'effective inertias' in the two models. That is, ETG zonal flows are 'heavy', while ITG zonal flows are 'light', and so ITG zonal flow generation should be much more effective (since the analysis assumes the scale separation $q\rho \ll 1$). Of course, any differences in saturation mechanisms for the two models will also be important for determining the dynamics and saturation levels of the zonal flows. In a like manner to $\delta(k_y)$, the damping term for the potential has been set so that all $k_y = 0$ potential modes are damped at the same rate ν (to mirror the expected form of zonal flow collisional damping [18, 33]) while finite k_y modes are damped as $\nu k^6 / (1 + k^2)$ (all pressure fluctuations are taken to be damped as χk^4). The advantage of studying these basic, prototypical fluid models of turbulence is that the governing equations are known exactly, and that analytic predictions of their dynamics are tractable and readily available for direct testing. These models also lend themselves to numerical simulation on desktop personal computers, which allows for direct, detailed tests of the analytic predictions with quite reasonable time and machine requirements.

The second step of this study was to investigate the impact of shear flows on nonlinear energy transfer in data from gyrokinetic simulations [35, 36] of ITG turbulence, and to compare these findings with the results from the simple fluid model. The gyrokinetic simulations represent the state of the art in numerical studies of plasma turbulence: far more detailed physics is included in these models, at the cost of greatly increased computational needs (both time and processor), and with generally less data available for post-processing.

3.1. Impact of shear flows on energy transfer in fluid models

It is generally believed that most of the crucial underlying physics for describing drift-wave turbulence can be captured in fluid models (such as those described above in equation (2)), even though kinetic treatments are usually required to accurately predict growth rates, frequencies, and eigenmode structure. However, when undertaking a complex study such as the one presented in this paper, it seems reasonable to begin with the simple models before progressing to more complex descriptions of the turbulence. Towards this end, a pair of simulations representing the ITG and ETG variants of the basic fluid model in equation (2) has been undertaken. The technical details of the simulations are as follows. Both simulations are two-dimensional, and assume periodic boundary conditions in x and y (equivalent to r and θ, respectively, in a toroidal geometry), with no gradients other than the implicit ones. Thus, the simulations are fully local and contain no magnetic geometry (in particular,

no magnetic shear) or profile relaxation effects. Given these conditions, one can simply define $k_y = 0$ modes to be zonal modes; modes with finite k_y are generically termed drift-wave or turbulent modes. The algorithm used is a pseudo-spectral hybrid Crank–Nicholson/RKW3 scheme with one-third aliasing scheme adapted from neutral fluid simulations [37], and all simulations were carried out on a 1 GHz PC laptop (in a true testament to advances in computing power). All simulations used a 256×256 grid (giving 171×86 modes), $L_x = L_y = 128\rho$, $\nu = \chi = 0.01$, $\varepsilon = 0.1$, $\eta = 3$, and a time step $= 0.001 L_n/u$. The simulations were run for a total time of $600 L_n/u$; data was saved every $\delta t = 1 L_n/u$. All results presented below have been averaged over the time range $T = [300:600]L_n/u$ which is taken to correspond to a saturated/slowly evolving state unless otherwise stated. Snapshots of the normalized electrostatic potential and pressure fluctuations in the saturated state (at $T = 500 L_n/u$) are shown in figure 2. Plots of total energy $E_{\mathrm{tot}} = \sum_k E_k$, $E_k = 0.5[(\delta(k_y) + k_\perp^2)|\phi_k|^2 + |p_k|^2]$ and flux $Q_k = 0.5 \, \mathrm{Im} \sum_k k_y p_{-k} \phi_k$ are presented in figure 3, time-averaged (over the steady-state period, denoted by $\langle \, \rangle_{\mathrm{T}}$) energy spectra $\langle E_k \rangle_{\mathrm{T}}$ in figure 4, and time-averaged zonal flow spectra $\langle |\phi_k|^2 \rangle_{\mathrm{T}}|_{k_y=0}$ for the ITG case in figure 5. One can clearly see the effects of the zonal flow suppression of the turbulence in the ITG case, relative to the ETG case, which does not exhibit zonal flow formation. All parameters other than $\delta(0)$ being equal, one sees that the ETG case saturates more slowly than the ITG case, and at a higher level (by roughly two orders of magnitude, as shown in figures 3(*a*) and (*b*)) relative to mixing length estimates. Also note that the (normalized) flux in the ETG case is much larger than the ITG case (again, by roughly two orders of magnitude) as shown in figures 3(*c*) and (*d*). More detailed statistical characterizations of the fluxes are described in section 5.
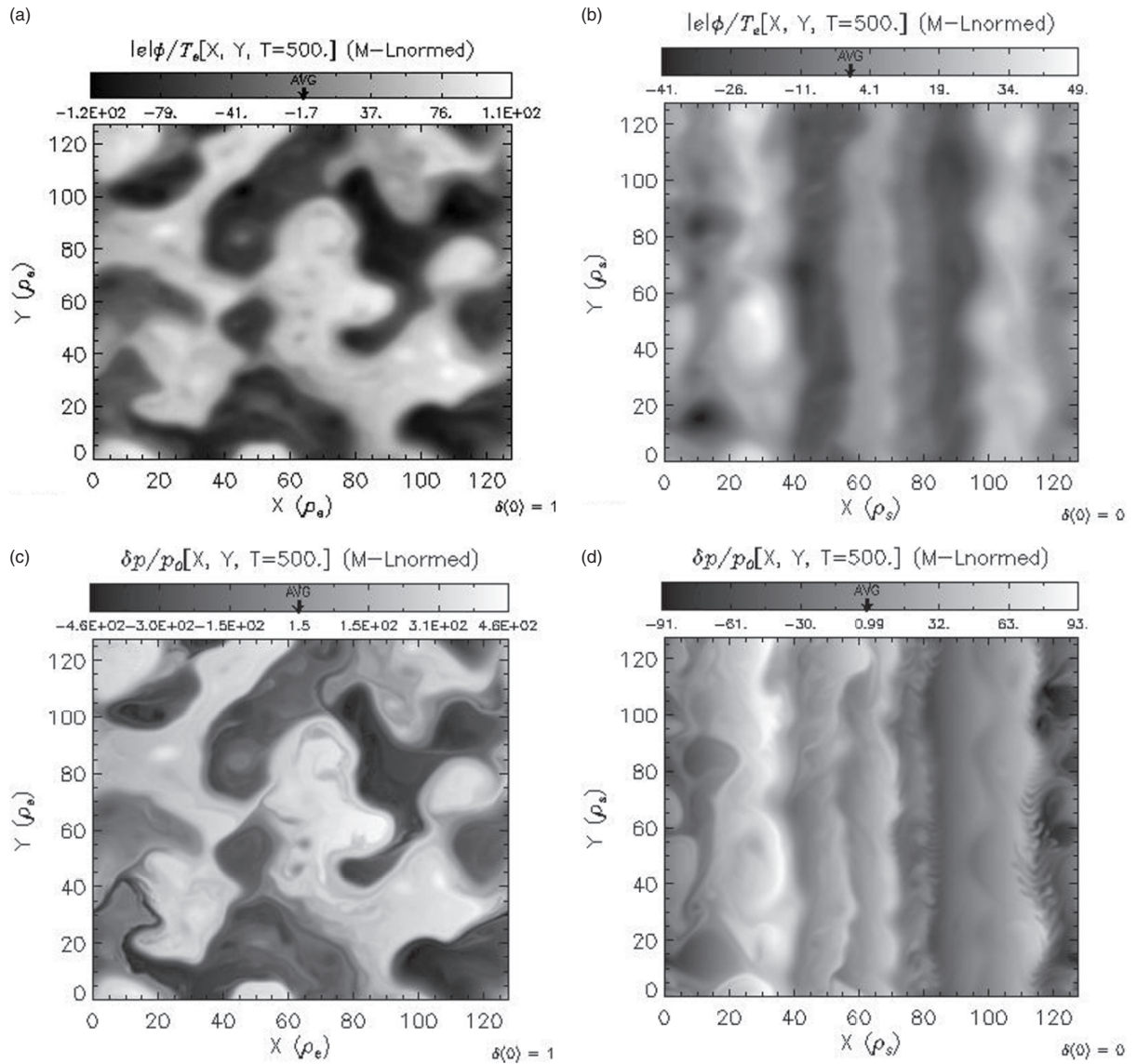
For both variants of the model, one can define two energy transfer functions, $T_k^\phi(k')$ and $T_k^p(k')$:

$$T_k^\phi(k') = \tfrac{1}{2} \hat{z} \cdot (\vec{k} \times \vec{k}')(|\vec{k}'|^2 - |\vec{k} - \vec{k}'|^2)$$
$$\times \mathrm{Re} \langle \phi_k^* \phi_{k-k'} \phi_{k'} \rangle, \quad (4)$$
$$T_k^p(k') = \hat{z} \cdot (\vec{k} \times \vec{k}') \mathrm{Re} \langle p_k^* \phi_{k-k'} p_{k'} \rangle.$$

$T_k^\phi(k')$ represents the transfer of kinetic energy $E_\phi = k^2 |\phi_k|^2$ from $\boldsymbol{k}'$ to $\boldsymbol{k}$, while $T_k^p(k')$ represents the transfer of internal energy $E_p = |p_k|^2$, and as such, will be the quantities focused upon in this section of this paper. With these definitions, one can rewrite the basic equations as

$$(\delta(k_y) + k_\perp^2) \frac{\partial}{\partial t} \left(\frac{\langle |\phi_k|^2 \rangle}{2} \right) = \varepsilon k_y \, \mathrm{Im} \langle p_{-k} \phi_k \rangle$$
$$- \nu(k) \langle |\phi_k|^2 \rangle + \sum_{k'} T_k^\phi(k'),$$

$$\frac{\partial}{\partial t} \left(\frac{\langle |p_k|^2 \rangle}{2} \right) = (1 + \eta) k_y \, \mathrm{Im} \langle p_{-k} \phi_k \rangle$$
$$- \chi k_\perp^4 \langle |p_k|^2 \rangle + \sum_{k'} T_k^p(k'), \quad (5)$$

$$\frac{\partial \langle E_k \rangle}{\partial t} = (1 + \eta + \varepsilon) k_y \, \mathrm{Im} \langle p_{-k} \phi_k \rangle - \nu(k) \langle |\phi_k|^2 \rangle$$
$$- \chi k_\perp^4 \langle |p_k|^2 \rangle + \sum_{k'} T_k^\phi(k') + \sum_{k'} T_k^p(k').$$
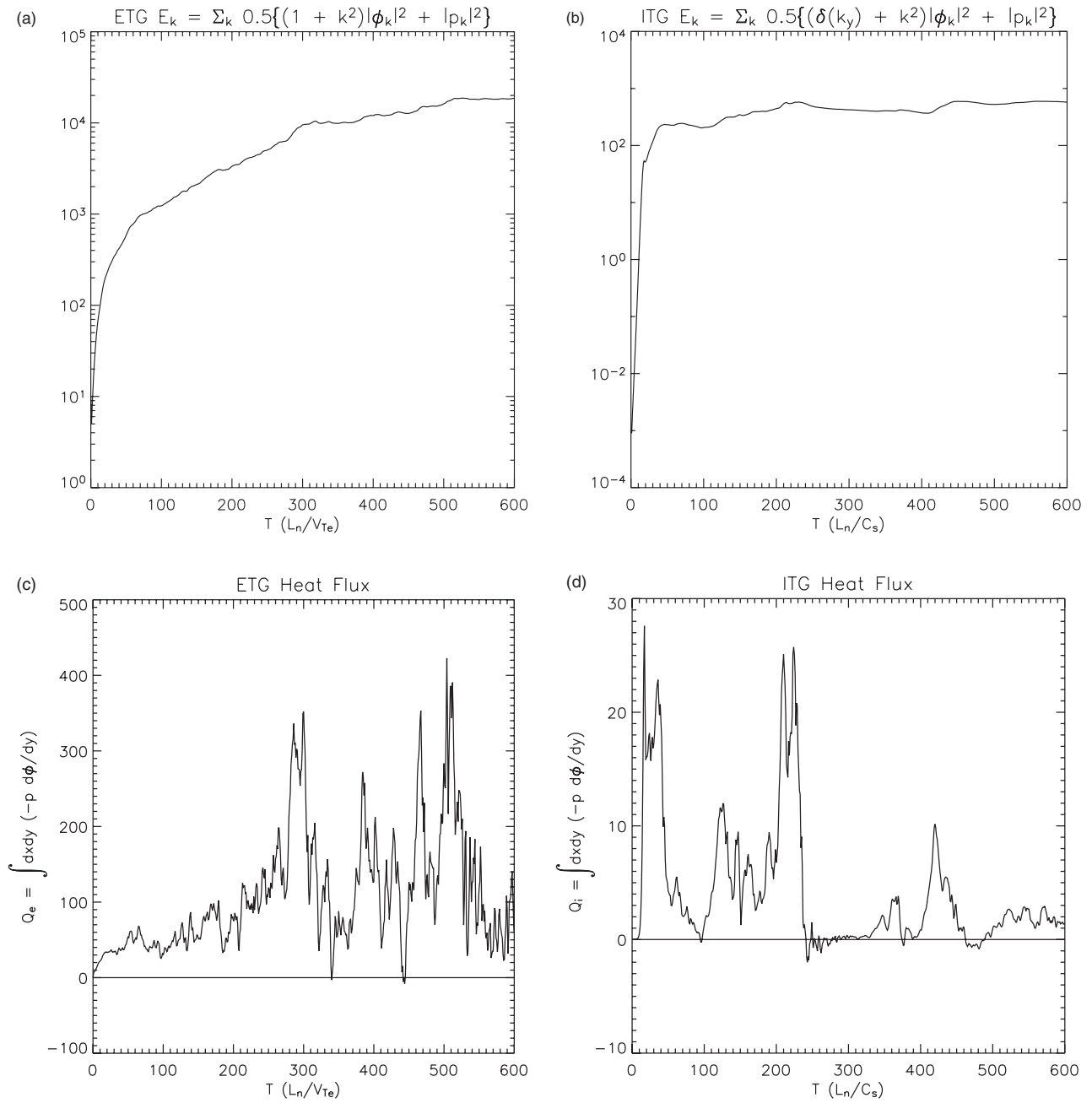
Figure 2. Snapshots of electrostatic potential and pressure fluctuations from saturated states of ETG (*a*) and (*c*), and ITG (*b*) and (*d*) fluid models.

To clarify the presented plots, note that a positive value of either transfer function would indicate that energy is being transferred from k' to k (an increase of energy in mode k), while negative values represent a transfer of energy to k' from k (decrease of energy in mode k).

An immediate problem that arises when studying these transfer functions is that of visualization: in their base form, they are four-dimensional functions of (k_x, k_y, k'_x, k'_y). In neutral fluids, a fundamental assumption of most turbulence theories is that the turbulence is isotropic, or close to it. This assumption suggests one method of reducing the dimensionality, which is to calculate $T_k(|\vec{k}'| \rightarrow |\vec{k}|)$, or the total transfer of energy from all modes with wavevector magnitude $|\vec{k}'|$ to modes with magnitude $|\vec{k}|$ [38]. One can view this approach as summing over all triads 'crossing' the boundary between $|\vec{k}|$ and $|\vec{k}'|$. However, in general plasma turbulence is not isotropic, particularly in the presence of shear flows. An alternate method of reducing the dimensionality

is to calculate $T_k^\phi(k')$ and $T_k^p(k')$ for specific values of k (i.e. looking at the energy transfer into and out of a specific zonal flow or turbulence mode). Selecting specific values of k allows one to take into account the anisotropy present in spectra, and it is hoped that by looking at the energy transfer for multiple modes, a cohesive and detailed picture of energy transfer can be developed. It should be noted, however, that the $T_k(|\vec{k}'| \rightarrow |\vec{k}|)$ approach has the advantage of presenting a 'global' picture of energy transfer (at the expense of detail for individual triplet interactions, and intensive computational costs); its usefulness in clarifying locality and directionality of bulk energy transfer is discussed later.

The first component of the fluid model analysis is to calculate $T_k^\phi(k')$ and $T_k^p(k')$ for several turbulent modes, all with $|k| = 0.5$; results for the $\vec{k} = (0, 0.5)$ mode (which are representative of the other $|k| = 0.5$ modes) are plotted in figure 6. For the ETG model (which does not exhibit zonal flow formation), we see that both $T_k^\phi(k')$ and $T_k^p(k')$

765

(a)

ETG $E_k = \Sigma_k \, 0.5\{(1 + k^2)|\phi_k|^2 + |p_k|^2\}$

(b)

ITG $E_k = \Sigma_k \, 0.5\{(\delta(k_y) + k^2)|\phi_k|^2 + |p_k|^2\}$

(c) ETG Heat Flux

(d) ITG Heat Flux

Figure 3. Total energy and flux for ETG (*a*) and (*c*), and ITG (*b*) and (*d*) fluid models.

are best described as interaction regions correlated with the largest amplitude modes (as indicated by the energy spectrum shown in figure 4(*a*)). Simply put, the dominant energy transfer involves the modes with the most energy. Within this region, one could characterize the interactions as roughly local (defined as $|\vec{k}| \sim |\vec{k}'| \sim |\vec{k} - \vec{k}'|$) in nature, isotropic (no particular values of k'_x or k'_y inside the interaction region are favoured), and without any clear net directionality of transfer (i.e. from k to smaller or larger k'). It is also useful to interpret the structure of the ETG transfer functions as 'base' cases, or controls, in that they reflect the structure of the couplings in the absence of significant shear flows. One can then ask how these structures change when shear flows are introduced (i.e. in the ITG case).

The primary change in the ITG model is the clear transfer or 'scattering' of energy between modes with wavevectors $\vec{k} = (0, 0.5)$ and $\vec{k}' = (\pm \delta k_x, 0.5)$ which is the expected signature of the strong shear flows, although there are also lower magnitude couplings similar to the ETG ('base') case. Note that the k'_x scattering does not have a clear directionality (the $k_x = 0$ drift-wave is both giving and receiving energy to/from the finite k_x modes). In addition, there is also significant energy transfer into and out of the zonal flow ($k_y = 0$) modes, reflecting the inherent symmetry of the transfer function. It is easy to see that $T_k^\phi(k') = T_k^\phi(k - k')$, and therefore if energy is 'scattered' to $\vec{k}' = (\pm \delta k_x, 0.5)$, an equal amount must be transferred to the zonal flow mode with $k_x^{ZF} = \mp \delta k_x$.
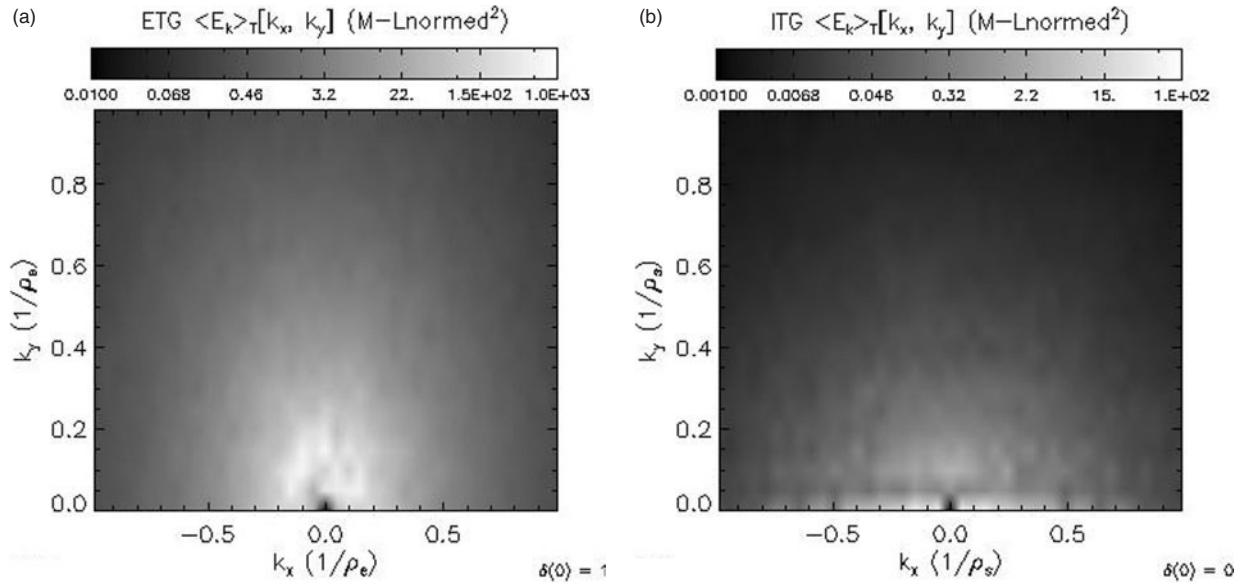
Figure 4. Time-averaged energy spectra for ETG (*a*) and ITG (*b*) fluid models.
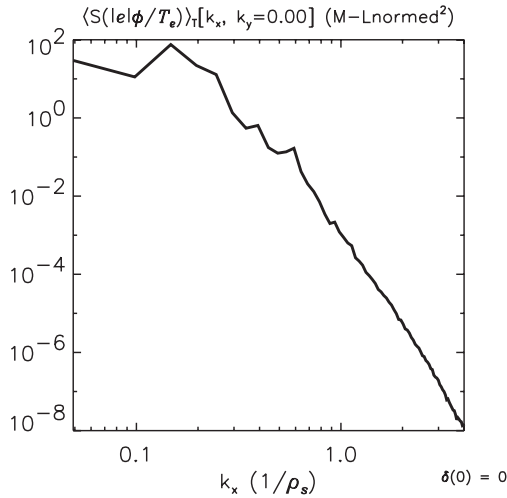

**Figure 5.** Zonal flow spectrum from fluid ITG model.

This symmetry explicitly demonstrates that the generation of zonal flows and zonal flow suppression of the turbulence by radial decorrelation (manifested as scattering in k_x) are dual facets of the same, single nonlinear process. $T_k^\phi(k')$ and $T_k^p(k')$ for the $\vec{k} = (0, 0.15)$ mode (where the spectrum of finite k_y modes peaks) is shown in figure 7; the results are essentially the same as those for the $\vec{k} = (0, 0.5)$ mode, suggesting that they are a universal feature of the transfer. Indeed, examination of energy transfer for other finite k_y modes (both with and without finite k_x) shows similar results. Another interesting result is that in general, the maximum values of $T_k^p(k')$ are $\geqslant 10 \times T_k^\phi(k')$. This difference can be understood by simply noting that the transfer functions depend on mode amplitudes, and the ratio of pressure fluctuations to potential fluctuation intensities $\langle |p_k| \rangle / \langle |\phi_k| \rangle$ is much greater than one; the coupling coefficient for $T_k^p(k')$ is also larger than that of $T_k^\phi(k')$ for wavenumbers less than one. However, it should be noted that the bicoherence and nonlinear phase relations between

the modes of the interacting triplet (analogous to the role of coherence and cross-phase in determining cross-spectra; see section 4 for a more detailed discussion of these quantities), in addition to the mode amplitudes, will also play a role in determining the energy transfer. An investigation of these quantities is ongoing. An important consequence of this result is that while analytic investigations have generally focused on $T_k^\phi(k')$ for both drift-waves and zonal flows rather than $T_k^p(k')$, overall transfer of drift-wave energy may be dominated by $T_k^p(k')$ rather than $T_k^\phi(k')$.

The energy transfer functions for the zonal potential and pressure have also been investigated; results for the dominant ($k_x = 0.15$) mode are shown in figure 8. Examination of $T_k^\phi(k')$ and $T_k^p(k')$ indicates that the majority of energy transfer involves drift-waves with $|k_y| < 0.3$, $-0.2 < k_x < 0.5$. Examination of the energy spectrum (figure 4(*b*)) suggests that this interaction region correlates with the core of the energy spectrum (which might be roughly characterized as $|k_x| < 0.4$, $|k_y| < 0.3$); the offset in k_x of the energy transfer interaction regions can be understood by noting that $k_x^{ZF} = 0.15$. The key features for $T_k^\phi(k')$ are that the strongest interactions seem to be (roughly) for $|k_x' - k_x^{ZF}| \sim 0.15$ (perhaps reflecting the k_x width of the drift-wave spectrum (figure 4(*b*))), and that there is both significant transfer into and out of the zonal flow. The transfer into the zonal flow fits the analytic picture in which drift-waves drive the zonal flow via transfer of kinetic energy (i.e. via the Reynolds stress). The transfer of energy from the zonal flow to the drift-waves is more surprising; one possible explanation would be that this transfer is a manifestation of an instability of the zonal flow (not inconsistent with the snapshot shown in figure 2(*b*), which suggests that Kelvin–Helmholtz like instabilities of the zonal flows may well be taking place); this hypothesis is explored further in section 3.2. It is also interesting to note that $T_k^p(k')$ indicates that internal energy is predominantly being transferred from $k_y > 0$ to $k_y < 0$ drift-waves (all values of k_y' are included to take into account the fact that for a fixed $\mathbf{k}$, there is no specific symmetry between the real parts of the $\mathbf{k}'$ and $-\mathbf{k}'$ triplets). To what extent this
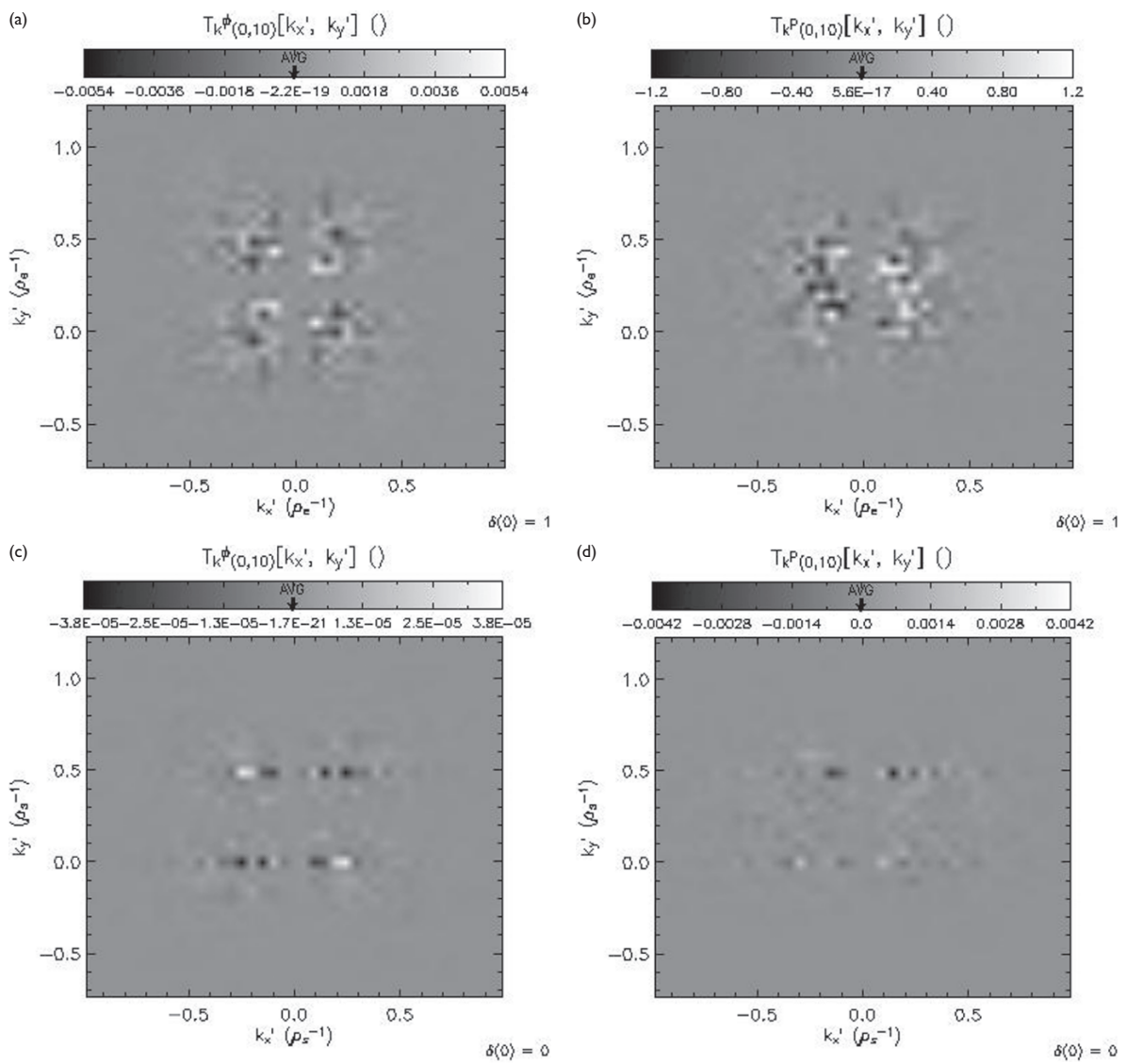
Figure 6. $T_k^\phi(k')$ (left column) and $T_k^p(k')$ (right column) for drift-wave with $k_x = 0$ and $k_y = 0.5$. (*a*) and (*b*) are from the ETG (no shear flows) case; (*c*) and (*d*) are from the ITG (shear flows present) case.
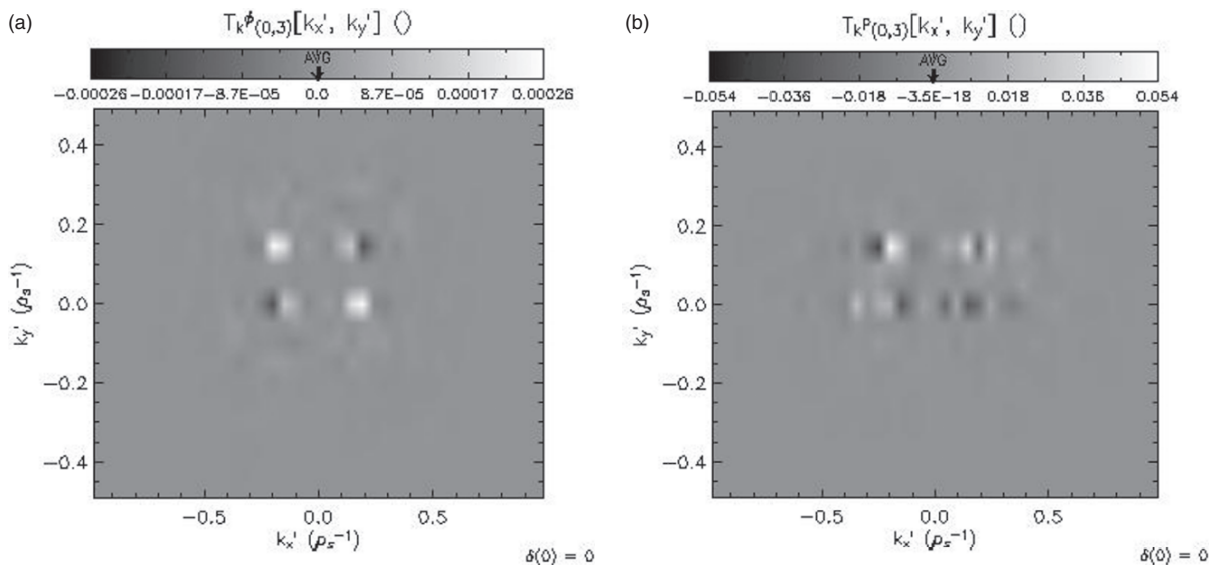
Figure 7. $T_k^\phi(k')$ (*a*) and $T_k^p(k')$ (*b*) for the $\boldsymbol{k} = (0, 0.15)$ ITG mode (where the fluid drift-wave spectrum peaks).
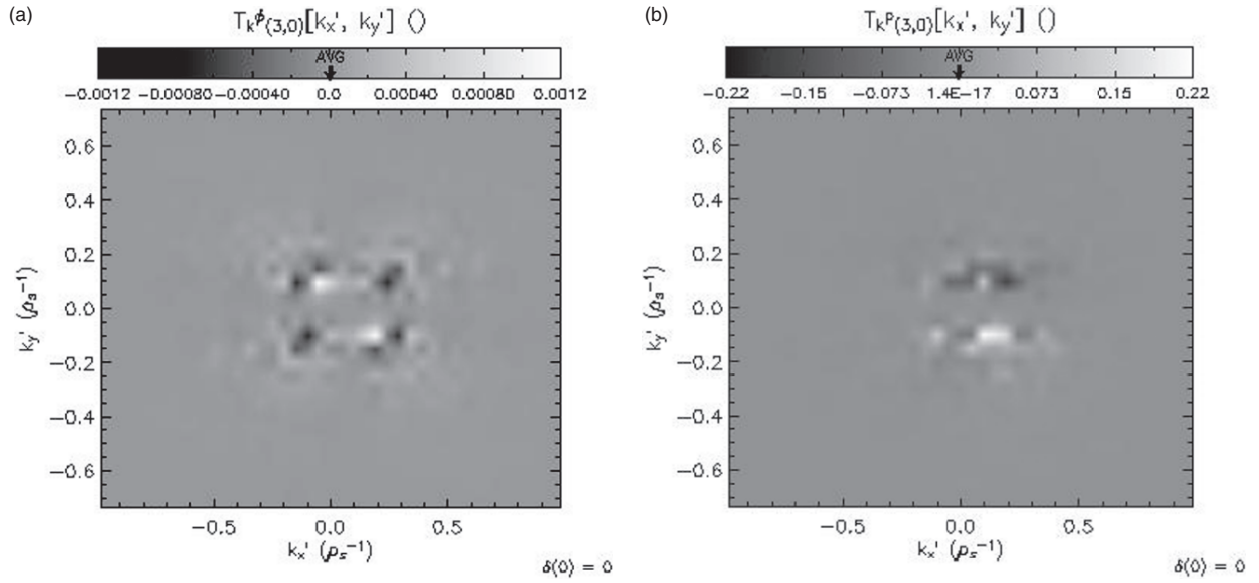
Figure 8. Plots of $T_k^{\phi}(k')$ (a) and $T_k^{p}(k')$ (b) for the dominant fluid ITG zonal mode ($k_x = 0.15$).

result simply reflects the symmetry properties of the coupling coefficient is unknown.
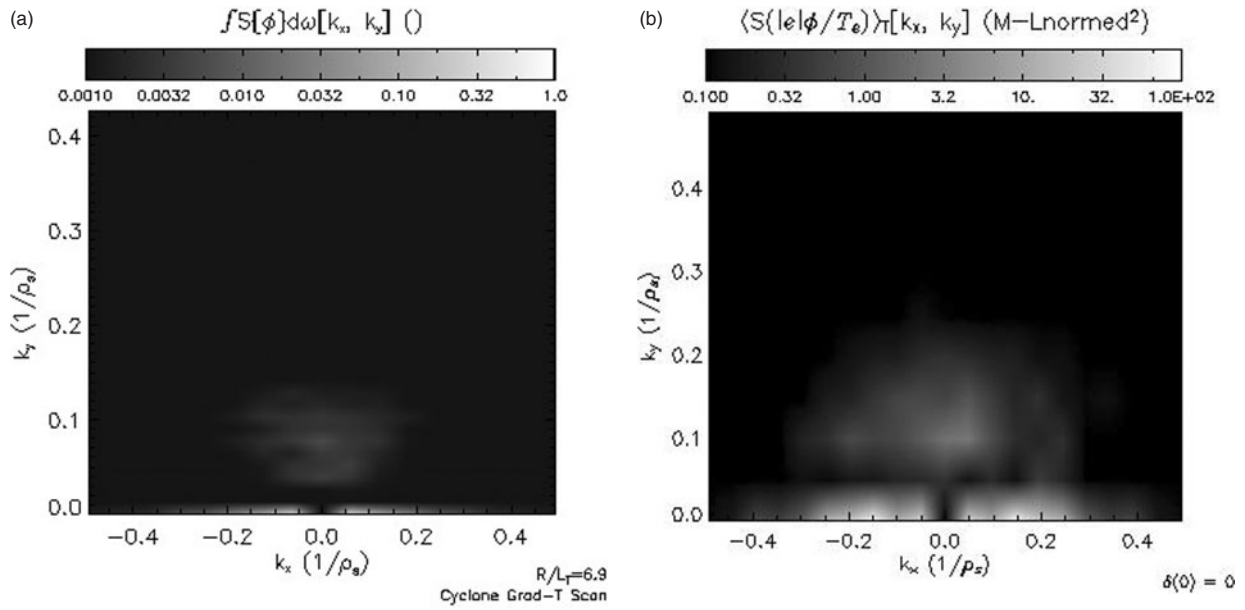
Several conclusions can be drawn from these results. First, in the absence of zonal flows, energy transfer is found to be weakly structured other than to occur in a local region, set primarily by the energy spectrum. The expectation that the effect of shear flows is to scatter energy in k_x at constant k_y, has been confirmed (i.e. that azimuthal and radial momentum are conserved in triad interactions), along with a correlated transfer of energy from the drift-waves to the zonal flow, demonstrating the inherently dual nature of zonal flow generation and drift-wave suppression. For energy transfer into/from a single mode, directionality of transfer is generally ambiguous. However, Carmargo *et al* [38] have calculated $T_k^n(k' \to k)$ ($= T_k^p(k' \to k)$, with $p \to n$) and $T_k^{\phi}(k' \to k)$ for the Hasegawa–Wakatani model [39] (which contains the same nonlinearities as the model considered here), and found that the global energy transfer remains predominately local, with global directionality in the predicted direction [16,17,40]: internal energy is locally transferred to smaller scales, while kinetic energy is transferred to larger scales (vorticity is also found to obey a local, forward cascade). Examination of $T_k^{\phi}(k')$ and $T_k^n(k')$ in the Hasegawa–Wakatani model reveals pictures strikingly similar to figures 6(a) and (b). It then may be that the appropriate view of energy transfer directionality (for like-scale interactions) is that it is an emergent property characterizing the sum of many individual triplet interactions. Calculations of $T_k^{\phi}(k' \to k)$ and $T_k^p(k' \to k)$ to study these global properties for the ITG/ETG model are currently in progress. $T_k^p(k')$ was found to be greater than $T_k^{\phi}(k')$, possibly depending simply on the ratio of p_k to ϕ_k, and the relative magnitudes of the coupling coefficients. This result suggests that consideration of internal energy transfer may be crucial to understanding the effects of shear flow on total drift-wave energy transfer, and that greater consideration of $T_k^p(k')$ may be needed to understand the full impact of zonal flows on turbulence. We note that as the effects of shear flows on internal energy transfer should be fairly insensitive to the source of the

shear flow, an experimental study of these dynamics could be feasible in an experiment with an imposed shear flow such as the controlled shear decorrelation experiment (CSDX) [41,42]. Finally, it was found that there is both kinetic energy transfer to zonal flows from drift-waves (of a nature in general accordance with analytic theory), and transfer to drift-waves from the zonal flows, which may be a manifestation of an instability of the zonal flows.
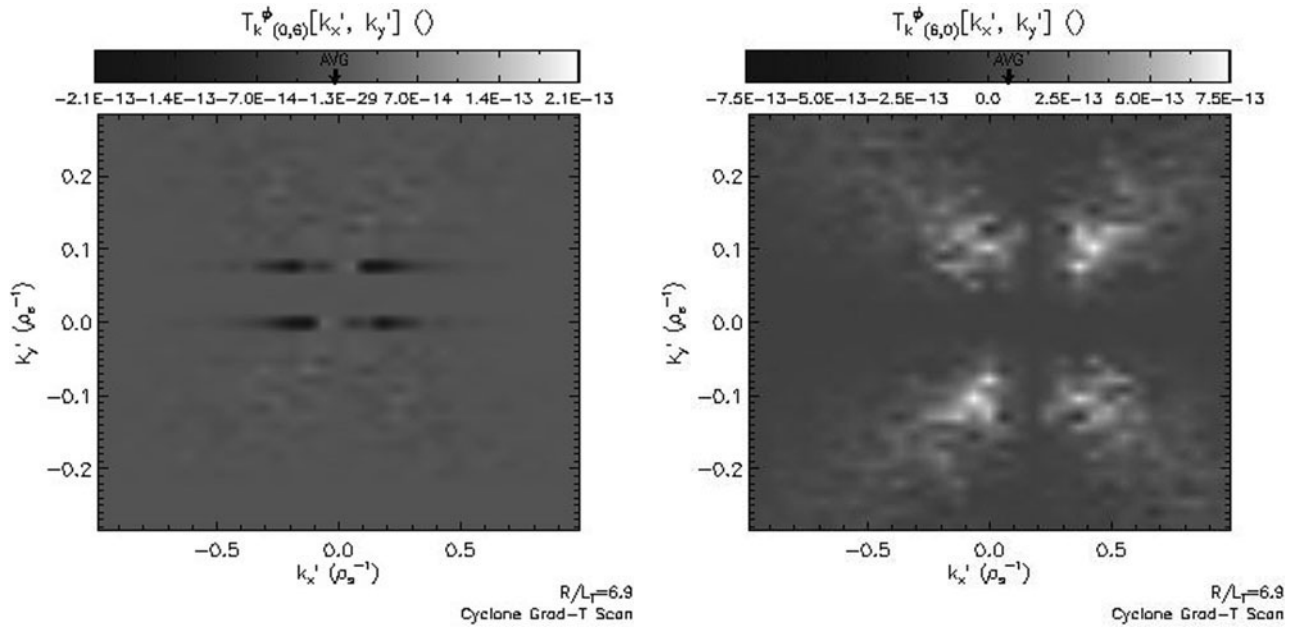
3.2. Impact of shear flow on energy transfer in gyrokinetic simulations

Having examined the effects of shear flow on energy transfer in the simple fluid models, this analysis is extended to address the data from a global gyrokinetic simulation by Candy *et al* [43] of ITG turbulence (specifically, the CYCLONE base case [44]). It should be noted that calculation of energy transfer requires knowledge of the appropriate coupling coefficient $\Lambda_{k,k'} (= \hat{z} \cdot (\vec{k} \times \vec{k}')$ in the case of internal energy transfer, or $\frac{1}{2}(\vec{k} \times \vec{k}') \cdot \hat{z}(|\vec{k}'|^2 - |\vec{k} - \vec{k}'|^2)$ for kinetic energy transfer). These coefficients are determined exactly by the fluid model used, but in reality only represent lowest-order (in $k\rho$) approximations to the full gyrokinetic couplings. Because attention in the section will be generally focused on modes with $|k\rho| < 1$, it seems reasonable to assume that the fluid coupling coefficients will be good approximations of the full gyrokinetic coefficients for this study. In addition, it should be noted that although an assumption is made on the structure of the coupling coefficient, this assumption has no impact on the bicoherence and phase relationships of the modes, which are also crucial in determining the energy transfer.

Availability of gyrokinetic data for post-processing limits the analysis to consideration of $T_k^{\phi}(k')$ at this time. For reference, the electrostatic potential spectrum for the gyrokinetic data (and the corresponding fluid ITG spectrum) is shown in figure 9. Energy transfer for drift-waves with $k_x = 0$ is investigated first; results are in figure 10.

769

(a)

$\int S[\phi]d\omega[k_x, k_y]$ ()

(b)

$\langle S(|e|\phi/T_e)\rangle_T[k_x, k_y]$ (M−Lnormed²)

R/L_T=6.9
Cyclone Grad−T Scan

δ⟨0⟩ = 0

Figure 9. Electrostatic potential spectra from gyrokinetic code GYRO (*a*) and fluid ITG model (*b*).

$T_k^{\phi}{}_{(0,6)}[k_x', k_y']$ ()

R/L_T=6.9
Cyclone Grad−T Scan

$T_k^{\phi}{}_{(6,0)}[k_x', k_y']$ ()

R/L_T=6.9
Cyclone Grad−T Scan

Figure 10. Calculations of $T_k^{\phi}(k')$ from GYRO code for a mode with $k_y = 0.18$ (where the gyrokinetic drift-wave spectrum peaks).

Figure 11. Calculations of $T_k^{\phi}(k')$ from the GYRO code for a zonal flow with $k_x = 0.18$.

Figure 10 (which shows $T_k^{\phi}(k')$ for a mode with $k_x = 0$, $k_y = 0.18$, corresponding to the peak value of the drift-wave spectrum) indicate that zonal flows clearly transfer energy from the $k_x = 0$ drift-waves to drift-waves with finite k_x and the same k_y as the original mode, and with an extended scattering width (roughly of the same width as the zonal flow spectrum). Figure 10 also clearly shows an equally strong and symmetrical transfer of energy to the zonal flow modes, which is again expected from the symmetry properties of $T_k^{\phi}(k')$; examination of $T_k^{\phi}(k')$ for other drift-waves provides similar results. It is interesting to note that in contrast to the fluid case, the directionality of the transfer due to 'scattering' (and equivalently, the transfer to the zonal flow modes) is uniformly out of the $k_x = 0$ drift-wave to the finite k_x drift-waves and zonal flows; there is no evidence for the transfer of energy from the zonal flow to the drift-waves as there was in the fluid case.

Figure 11 shows $T_k^{\phi}(k')$ for a zonal flow with $k_x = k_x^{ZF} = 0.18$ (the dominant zonal flow mode). There is a clear transfer of energy from a broad spectrum of drift-waves into the zonal flow; the transfer is uniformly into the zonal flow, in agreement with the results shown in figure 10. Some insight into the structure of the transfer can be gained by noting that for a

zonal flow mode, the coupling coefficient can be rewritten as

$$\Lambda^{\phi}_{k,k'} = \frac{1}{2}(\vec{k}^{\text{ZF}} \times \vec{k}') \cdot \hat{z}(|\vec{k}'|^2 - |\vec{k}^{\text{ZF}} - \vec{k}'|^2)$$

$$= (k_x^{\text{ZF}})^2 k_y' \left(k_x' - \frac{k_x^{\text{ZF}}}{2}\right). \tag{6}$$

Therefore, any modes with $k_y = 0$ (other zonal flows), or $k_x = k_x^{\text{ZF}}/2$ cannot exchange energy with the zonal flow. When combined with the size of the drift-wave spectrum (figure 9(a)), the transfer into the zonal flow can be interpreted as a broadband Reynolds-stress drive. Compared to the fluid ITG case, what is particularly striking in the gyrokinetic results is the much clearer directionality of the interactions between the drift-waves and zonal flows. One possible explanation for the relative 'clarity' is that zonal flows are relatively much stronger in the gyrokinetic case (most likely because of stabilization with respect to large-scale Kelvin–Helmholtz type instabilities [19]), and thus convection of drift-wave energy by zonal flows is much stronger in the gyrokinetic case; this issue is further explored later. However, this difference cannot be the entire story, as simply changing the magnitudes would not affect the directionality of the transfer, only its magnitude; a change in directionality could only be accomplished by a change in the relative phases of the interacting modes (more specifically, the biphase) of a particular triplet (this restriction follows directly from the definition of $T_k^{\phi}(k')$). Another possible explanation could come from the fact that fluid closures are inherently imperfect models of the full phase-space structure of the distribution function; this issue has been explored by Watanabe and Sugama [45].

Having studied energy transfer in both fluid and gyrokinetic models, it is natural to try and find a universal description of the results. These results suggest an intriguing picture of global energy transfer. They support the expectation that in the saturated state, zonal flows are sustained by an inverse transfer of kinetic energy from drift-waves, while at the same time 'scattering' drift-wave energy in k_x at fixed k_y. However, the results also indicate that there can be
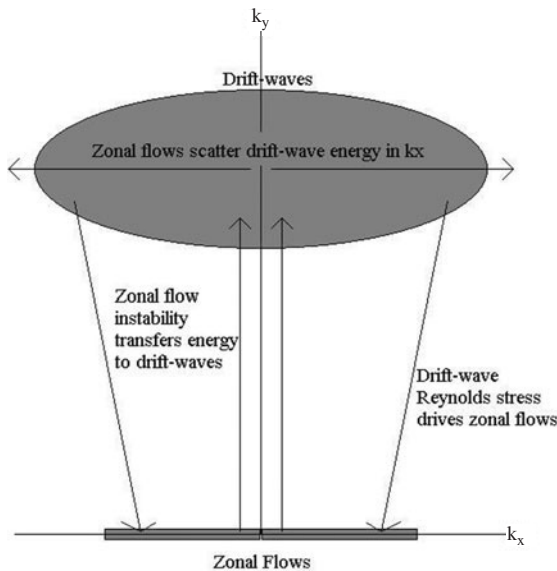

Figure 12. Heuristic model of energy transfer loop.

significant transfer of energy from zonal flows to turbulence! One particularly interesting question is whether the transfer of energy transfer from zonal flows to drift-waves is a signature of some instability of the zonal flows (possibly limiting zonal flow growth). If one were to suppose this hypothesis to be the case, these results would suggest that energy is exchanged between drift-waves and zonal flows in a 'loop' (a heuristic diagram is shown if figure 12; also see figure 2 of Kim and Diamond [46] for a variant of the model described here): drift-waves transfer energy to zonal flows via the Reynolds stress, while at the same time the zonal flows may give energy back to the drift-waves via an undetermined nonlinear mechanism; simultaneously drift-wave energy is scattered in k_x by the zonal flows. Coupled with a low level of residual linear instability and damping of high k drift-waves (into which energy should also be scattered) as sources and sinks, a very intriguing potential model for the saturated state of drift-wave turbulence emerges. It should be noted that this model is by no means incompatible with earlier models of saturation levels for zonal flows and turbulence (in which zonal flows saturate only via collisional damping), but rather builds upon them to include the possibility (and implications) of higher-order and nonlinear instabilities as saturation mechanisms for zonal flows. Generally, one could write a more generalized set of equations describing zonal flow–drift-wave interactions, in the form

$$\frac{\partial U}{\partial t} = \gamma_{\text{mod}}(\langle N \rangle)U - \gamma_{\text{linear}}^{\text{ZF}} U$$

$$- \gamma_{\text{flow}}(\langle N \rangle, V_{\text{ZF}}, \vec{r})U + [\text{noise}],$$

$$\frac{\partial \langle N \rangle}{\partial t} - \frac{\partial}{\partial k_r} D(U) \frac{\partial \langle N \rangle}{\partial k_r} \tag{7}$$

$$= (\gamma_{\text{lin}}(\vec{k}) + \gamma_{\text{NL}}(\phi_q, \vec{k}, \ldots))\langle N \rangle - \Delta\omega(\vec{k})\langle N \rangle^2$$

(see equations (25a) and (25b) of [3] for a similar model describing the generation and saturation of radially extended convective cells by turbulence); the notation used is the same as in equation (1). In this extended model, both linear damping ($\gamma_{\text{linear}}^{\text{ZF}}$, due to both magnetic pumping and Rosenbluth–Hinton collisions [47]) and flow instability (γ_{flow}) contribute to the zonal flow damping rate, and there is feedback on the drift-waves from both linear flow shear ($D(U)$) and zonal flow instability (γ_{NL}). It is crucial here to realize then that the zonal flow-damping rate will itself be a sensitive function of zonal flow profile, collisionality, and drift-wave amplitude.

It is also important to discuss the physics and mechanisms of zonal flow feedback to drift-waves carefully. First, it is well-known that magnetic shear [48], Landau damping [49], and other geometric and kinetic effects will considerably reduce the virulence of the classical Kelvin–Helmholtz type instability, if not stabilize it outright (also see [34]). Thus, it is unlikely that in a realistic tokamak-geometry, γ_{flow} will manifest itself as a 'macro' Kelvin–Helmholtz type instability which causes vortex sheet roll-up and destroys the zonal flow; however, this kind of instability could be occurring in simple shearless slab models (such as the fluid models discussed in this paper). Rather, more subtle mechanisms are likely, including possibly:

(1) Noise-induced flow defects and their relaxation.
(2) Modulational instability of non-axisymmetric zonal modes.
(3) Drift-wave induced viscosity.
(4) Drift-wave wave-packet trapping.

We comment on each of these below.

771

While zonal flow potential vorticity profiles have not been studied in detail, it seems likely that in the presence of drift-wave interaction, noise emission will induce small bumps or 'defects' [50] in the potential vorticity profile, thus producing an instantaneous profile with many local inflection points. The relaxation of such defects may then be thought of as 'micro' Kelvin–Helmholtz mode turbulence, which will transport zonal flow mean potential vorticity (thus acting as a turbulent viscosity), and which extracts energy from the zonal flow and returns it to the drift-wave background. Moreover, in the presence of such drift-wave noise, it is not even necessary for the defect-resonant Kelvin–Helmholtz mode to be linearly unstable! Indeed, as is well-known, weakly damped modes can be quite effective mechanisms for turbulent transport when excited by noise [51]. In this picture, then, the instantaneous zonal flow profile may be thought of as a kind of self-organized criticality, which evolves due to noise and local relaxation [52]. The effective viscosity could be calculated using standard methods of mean-field turbulent hydrodynamics (see, e.g. [51, 52]). As discussed in [46], another possibility is the generation of low m flows via modulational processes similar to those, which generate zonal flows. Such low m modes transport zonal flow momentum and relax the flow profile, thus providing a vehicle for energy feedback to drift-waves. As they are comparatively weakly damped, strong drive is not required to make such a process significant. Further details of this mechanism can be found in [46]. Of course, the ambient drift-wave turbulence can itself produce a turbulent viscosity by $E \times B$ transport of zonal flow potential voriticity. A turbulent viscosity may be estimated by standard quasi-linear methods. It is also possible that more complex nonlinear phenomena, such as the trapping of a drift-wave wavepacket, could affect zonal flow dynamics (see [20–23] for initial studies of this phenomenon).

To answer the obvious question of how to distinguish which of these mechanisms is actually at work, it would be very instructive to:

(1) scan the behaviour of $T_k^\phi(k')$ for zonal flows as a function of $(\nabla T - \nabla T_C)/\nabla T_C$,
(2) study the spatial structure of zonal flows, at high spatio-temporal resolution.

Here, (1) should distinguish between varying dependences on the fundamental system drive and (2) should elucidate the possible role of defects and their interactions.

This proposed model also underscores the need for a better understanding of zonal flow saturation mechanisms; initial efforts on this subject can be found in [19, 34, 46]. In particular, a better understanding of the competition between macro tertiary instabilities, collisional damping, nonlinear spectral feedback, and the newly proposed mechanisms (flow defects, non-axisymmetric zonal modes, turbulent viscosity, and wave-packet trapping) is needed. The proposed model also raises several other questions/problems. Foremost, if the observed transfer is in fact an instability of the zonal flows, is this instability what is saturating the zonal flow. It is possible to imagine, for example, that the zonal flows might be saturating via linear damping mechanisms, but still be weakly unstable to various instabilities (which could be saturation mechanisms in the absence of collisions), or the formation of defects as discussed earlier. It should also

be noted that for some of the newly proposed zonal flow relaxation mechanisms (such as flow defects), 'instability' may not be the appropriate characterization, as they may not lead to the destruction of the mean zonal flow profile. A second, perhaps more philosophical question, is whether there is any meaningful distinction between a $k_x = 0$, finite k_y mode driven by zonal flow instability or relaxation (the so-called 'tertiary instability' mode) and a $k_x = 0$ drift-wave. Third, it should be noted that the feedback of zonal flows on drift-waves might induce spatial spreading of drift-wave intensity, causing 'fast transport' or 'nonlocality' phenomena. A key difficulty for developing this hypothesis has been how to introduce a spatially nonlocal mechanism for energy transfer from zonal flows to drift-waves; we note that zonal flow defects may provide just such a mechanism. Finally, it seems quite possible that the existence of multiple zonal flow instabilities and relaxation methods could explain some of the differences between the fluid and gyrokinetic results, especially if combined with differences in the spectra (i.e. the fluid spectrum peaks at lower k_y than the gyrokinetic model) and physics contained in the models. In particular, although both models exhibit zonal flow formation, differences in the physics included (particularly geometry effects) should greatly affect the nature of the zonal flow dynamics, which will have an impact on the relative saturation levels of the zonal flows, which in turn will affect the relative magnitudes (and directionality) of zonal flow–drift-wave couplings.

4. Bicoherence studies and connecting to experiment

While it is important to understand the nonlinear behaviour exhibited by analytic and computational models of turbulence, such an understanding is of limited practical use if it cannot be connected to the experiments the models are expected to describe. Bispectral analysis [53–55] represents a possible way of connecting and relating the nonlinear dynamics in experiment, simulation, and theory. The bispectrum of three (real) signals X, Y, and Z is defined as

$$S(k_1, k_2) = \langle X_{k_3}^* Y_{k_1} Z_{k_2} \rangle, \tag{8}$$

where $\vec{k}_1 + \vec{k}_2 = \vec{k}_3$, and the brackets represent an ensemble average. The relation between the bispectrum and energy transfer is clear: the energy transfer functions $T_k(k')$ are the coupling coefficient times the real part of the appropriate bispectrum (i.e. $S_k^\phi(k') = \langle \phi_k^* \phi_{k'} \phi_{k-k'} \rangle$ for $T_k^\phi(k')$). The bispectrum can be decomposed into a bicoherence, biphase, and quantities related to mode amplitudes. The bicoherence $b(k_1, k_2)$ is defined as

$$b(k_1, k_2) = \frac{|\langle X_{k_3}^* Y_{k_1} Z_{k_2} \rangle|}{\sqrt{\langle |X_{k_3}|^2 \rangle} \sqrt{\langle |Y_{k_1} Z_{k_2}|^2 \rangle}} \tag{9}$$

and the biphase $\Theta(k_1, k_2)$ as

$$\Theta(k_1, k_2) = \tan^{-1} \left(\frac{\text{Im} \langle X_{k_3}^* Y_{k_1} Z_{k_2} \rangle}{\text{Re} \langle X_{k_3}^* Y_{k_1} Z_{k_2} \rangle} \right). \tag{10}$$

There is a natural correspondence between bicoherence/biphase and the coherence and cross-phase. Indeed, the choice

of bicoherence normalization is such that if one were to define a new field $X'_{k_3} = Y_{k_1} Z_{k_2}$, the bicoherence would reduce to the definition of the $X - X'$ coherence, and the biphase the $X - X'$ cross-phase. In particular, also note that the values of the bicoherence are restricted to lie between zero and one (inclusively), just as values of the coherence are.

Since the bicoherence provides a direct measurement of nonlinear coupling, it represents a potential avenue for making contact between experimental analysis and analytic/computational predictions of nonlinear dynamics (interpretation of the biphase without knowledge of the coupling coefficient is generally more complex). By this statement, we mean that the bicoherence can provide a quantitative measure of the strength of nonlinear correlation, just as the coherence provides a quantitative measure of linear correlation. For instance, a bicoherence with a value near one indicates the modes of a particular triplet are strongly correlated, while a coherence with a value near one indicates a strong correlation between a pair of modes/signals/fluctuations, etc. However, just like the coherence, the bicoherence should not be regarded as a definitive measure of energy transfer, which will depend on the coupling coefficient, mode amplitudes, and biphase, just as a (quadratic) flux depends not only upon the coherence, but also mode amplitudes and cross-phase. Nonetheless, the bicoherence represents a (relatively) easily understood statistic, which provides information about the nonlinear dynamics of the system. Therefore, one might attempt to make a comparison between the bispectra or bicoherences measured in experimental data and a simulation of that experiment, or even analytically predicted values; for instance, initial analytic work by Diamond and co-workers [24] suggests that the bispectrum relevant for zonal flow generation by modulational instability of a broad drift-wave spectrum should take the form:

$$\langle \tilde{V}_r^{\mathrm{DW}} \tilde{V}_\theta^{\mathrm{DW}} \phi_q^{\mathrm{ZF}} \rangle = 2q_r^2 c_s^4 \frac{k_\theta^2 \rho_s^2}{(1 + k_\perp^2 \rho_s^2)^2} \frac{R_{\vec{k},q}}{\Omega_{\mathrm{ci}}} k_r \frac{\partial \langle N \rangle}{\partial k_r} |\phi_q^{\mathrm{ZF}}|^2 \tag{11}$$

(using the notation of sections 2 and 3) from which it follows that the bicoherence would be given by:

$$b(\vec{k}, q_r) = 2q_r^2 \rho_s^2 \frac{k_\theta^2}{|k_r k_\theta|} \left| R_{\vec{k},q} \Omega_{\mathrm{ci}} \frac{k_r}{\langle N \rangle} \frac{\partial \langle N \rangle}{\partial k_r} \right| |\phi_q^{\mathrm{ZF}}|. \tag{12}$$

The primary difficulty of such a comparison is that experimental data generally has significant temporal range with very limited spatial resolution, while computational results are the opposite: information at many physical points but for a comparatively short period of time. The problem can be reduced to finding a way of connecting frequency-based representations of turbulence (experimental results) with wavenumber-based representations (computational/analytic results). In this section, we present the results of a simple 'thought experiment' which attempts to connect these representations via studying the bicoherence in a heuristic computational model of published experimental results.

The experimental results to be modelled are presented by Moyer et al [56], who have reported on the temporal dynamics of bicoherence near the separatrix during a spontaneous low–high (L–H) confinement transition in the DIII-D machine

(also see Tynan et al [57] and Holland et al [58] for more discussions of these results). In this research, it was found that just before a L–H transition, there was a marked change in the bicoherence calculated from floating potential and ion saturation current measurements using a Langmuir probe array; no changes or dynamics were observed when the probe was located several centimetres outside the separatrix during a comparable discharge. In addition, the bicoherence inside the separatrix suggested that there was strong coupling between a range of frequencies ($100\,\mathrm{kHz} < f < 1000\,\mathrm{kHz}$), and very low frequencies ($f < 50\,\mathrm{kHz}$); this signature was shown to be consistent with the idea that the L–H transition may be triggered by nonlinearly generated zonal flows which suppress the turbulence long enough for the transport barrier to develop [56, 59, 60].

To make an initial attempt at contact, a numerical experiment was undertaken, in which zonal flows are suppressed, and the turbulence is allowed to evolve into a saturated state; zonal flow generation was then 'turned on'. These simulations are a simple attempt to mimic a transition from a highly turbulent regime to a shear-flow dominated one, similar to the conditions examined in [56]. To accomplish this, the potential and pressure fluctuation fields from the ETG-like equations (in which zonal flows do not form) at $T = 400 L_n/u$ are taken as initial conditions. Zonal flows are 'turned on' by simply setting $\delta(0) = 0$, and allowing the model to evolve; the flows appear rapidly, and the system evolves towards a new nonlinear equilibrium. The underlying hypothesis of this investigation is that in both the experimental results and the numerical studies here, zonal flow generation is spontaneously triggered in saturated drift-wave turbulence; one might then ask how the bicoherences in the two cases compare as a (initial) comparison of the nonlinear dynamics. A similar numerical experiment was previously undertaken by Lin and co-workers (reported on in Diamond et al [3]) to demonstrate the role of zonal flows in regulating turbulence.

Total energy E_{tot} (as defined in section 3) for the two cases (transition to shear-flow dominated, and the 'base' turbulent case) is shown in figure 13, as is the kinetic energy of the zonal modes $E_k^{\mathrm{ZF}} = \sum_{k_x} k_x^2 |\phi_k^{\mathrm{ZF}}|^2$. To make contact with experiment, the data is divided into segments of length $25 L_n/u$ (i.e. $T = 400$–$424 L_n/u$, 425–$449 L_n/u$, etc). For each segment, the k_x-integrated values of the electrostatic potential, $\bar{\phi}(k_y, t) = \sum_{k_x} \phi(k_x, k_y, t)$ (equivalent to Fourier transforming the field only along y at $x = 0$) are calculated, which are then used to calculate the (squared) bicoherence as

$$b^2(k_{y1}, k_{y2}) = \frac{|\langle \phi^*(k_{y1} + k_{y2}, t)\phi(k_{y1}, t)\phi(k_{y2}, t)\rangle|^2}{\langle |\phi(k_{y1} + k_{y2}, t)|^2\rangle \langle |\phi(k_{y1}, t)\phi(k_{y1}, t)|^2\rangle}, \tag{13}$$

where the brackets denote a time average (conventionally, $b^2(k_{y1}, k_{y2})$ rather than $b(k_{y1}, k_{y2})$ is often presented in the literature; we do so here to maintain continuity with existing, published results). The idea here being that one might hope that k_y of the k_x-integrated potential fluctuations could be a suitable proxy for frequency of the experimentally measured fluctuations, based on ideas such as the 'frozen-flow' hypothesis. As discussed in [56], the frozen flow hypothesis is valid when the propagation time δt through the sampling volume d is short relative to the auto-correlation time τ_{corr};
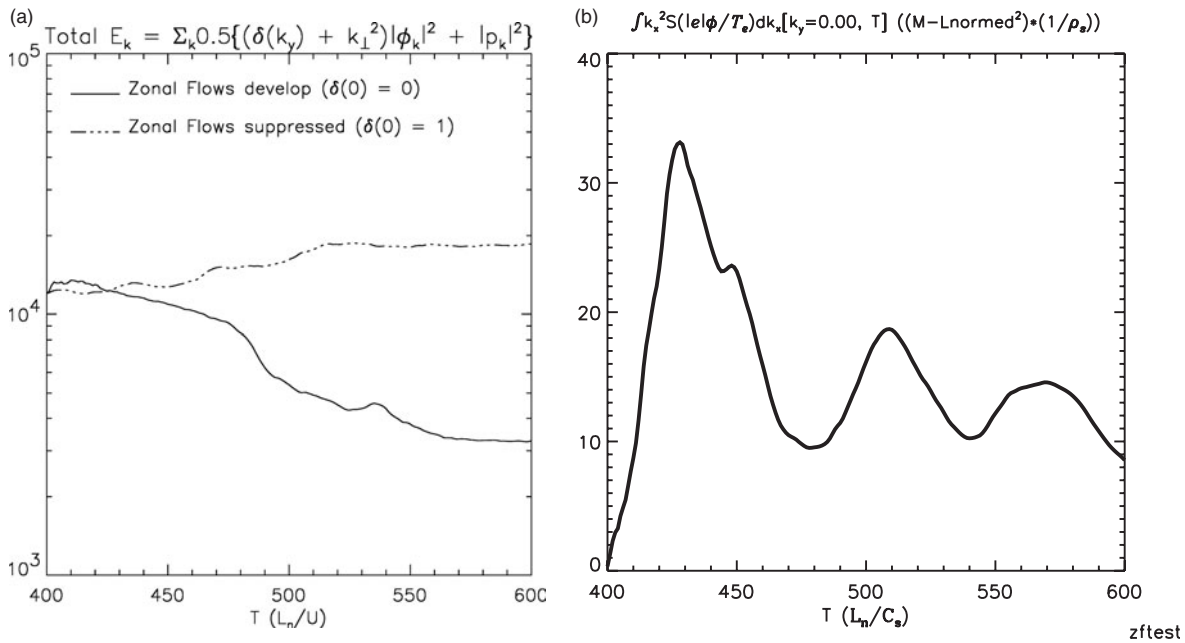
Figure 13. Total energy for base and shear flow cases (*a*) and evolution of zonal flow energy (*b*).
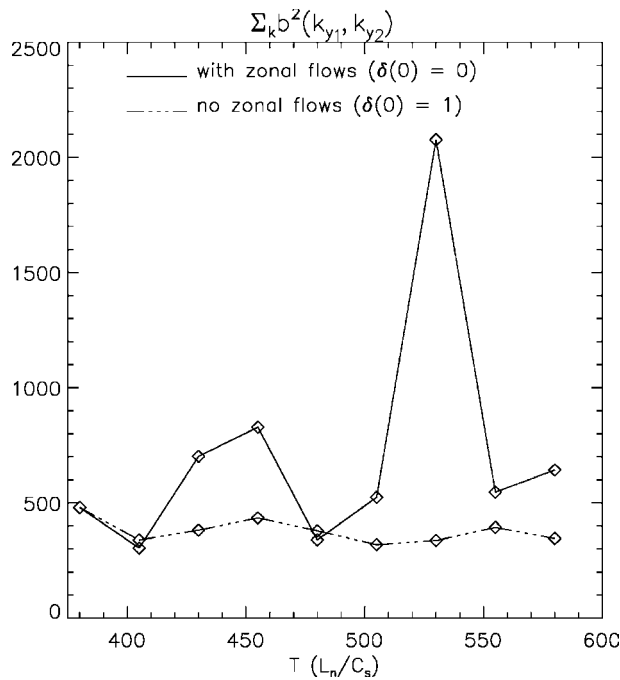
Figure 14. Total b^2 for base and shear flow cases. Solid lines indicate time sections used for calculating each data point.

in essence, that the eddies remain coherent and correlated as they pass through sampling volume. Under this condition, which is often satisfied in tokamak experiments, which exhibit L–H transitions and/or internal transport barrier formation, the frequency can be linearly related to the poloidal wavenumber (equal to k_y in the simulations) via the measured phase velocity v_θ. Thus $k_y \propto f$ in both L-mode and H-mode, and so our comparison of the wavenumber-space and frequency-space bicoherences should provide both a reasonable and meaningful qualitative comparison between simulation and experiment.

The bicoherence is calculated for both the zonal flow case and the case with zonal flows suppressed. The total $b^2 = \sum_{k_{y1}, k_{y2}} b^2(k_{y1}, k_{y2})$ for each time segment is plotted in figure 14, similar to figure 4 of Moyer *et al*. Comparing with the energy history plots, one can see that the zonal flow evolution dynamics clearly impact the dynamics of total bicoherence, but quantifying the exact connection is a harder question. However, these results and those published in Moyer *et al* seem qualitatively quite similar, in that for the case where shear flows are evolving, strongly correlated temporal dynamics in the bicoherence are seen, whereas the cases without evolving flows show steady, lower levels of total bicoherence. For a more detailed comparison with Moyer *et al*, $b^2(k_{y1}, k_{y2})$ from the $T = [450 : 474]$ and $T = [525 : 549]$ segments for both the zonal flow and base case are shown in figure 15. For the zonal flow case, the structure of the bicoherence in the various segments is generally similar to the $T = [450 : 474]$ segment, while the widespread structure of $T = [525 : 549]$ is unique to that time segment. The base cases all show roughly the same structure (strong local coupling between the lowest k_y modes). The banding structures of the $[450:479]$ segment are intriguingly similar to figures 3(*b*) and (*d*) from Moyer *et al* while the results for the base case are quite similar to the structure exhibited by the bicoherence when well separated from the L–H transition. These structures indicate strong coupling between relatively high values of k_y (based on where spectra indicate the bulk of the energy is located) and very low values of k_y; that is, significant nonlocal coupling between high-wavenumber modes and very low wavenumber modes. Note that the $k_{y2} = 0$, $-k_{y1}$ axes have been intentional set to zero (as they are for the plots in Moyer *et al*). If they are not, they are ~ 1 for all values of k_{y1}. This is a consequence of the fact that the mean value of ϕ (represented by $k_y = 0$) is slowly or not evolving at all. An important open question is how this relates to turbulence–zonal flow coupling, as zonal flows have $k_y = 0$. It is also interesting that the interactions are generally
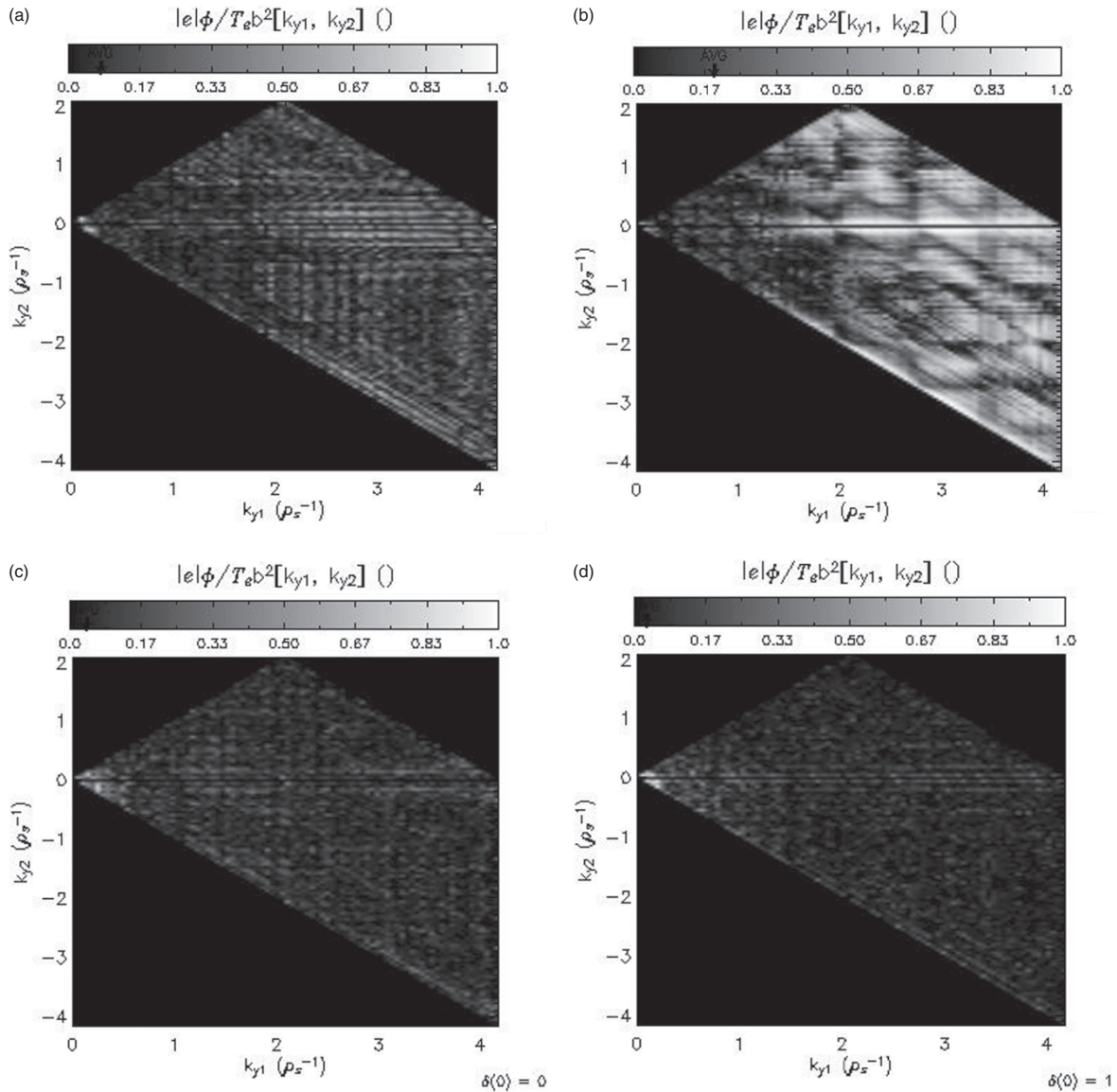
Figure 15. k_y resolved b^2 from shear flow (*a*) and (*b*), and base (*c*) and (*d*) cases. Plots (*a*) and (*c*) correspond to $T = [450 : 474]$, while (*b*) and (*d*) correspond to $T = [525 : 549]$.

for much higher k_y than one might guess from looking at the (k_x, k_y) spectrum, which is also in agreement with the results of [56]. Finally, it should be noted that the work presented in [56] is from the edge of the DIII-D tokamak, which raised the possibility that interactions between geodesic acoustic modes (GAMs) and the turbulence [61,62], rather than zero frequency zonal flows, was being observed. However, the model used here does not contain GAMs, which supports the idea that the shearing of the turbulence does not depend sensitively on the magnetic geometry used (which GAMs do depend on, being driven by poloidal asymmetries).

This simple experiment provides a very interesting point for furthering the contact between experiment, simulation, and theory. Understanding the structure and dynamics exhibited by the bicoherence remains an open problem, particularly why the bicoherence peaks at high k_{y1}/f_1. The qualitative similarity between the numerical and experimental results indicate that developing more rigorous methods of connecting the wavenumber-space and frequency-space

representations would be of great utility in connecting the analytic/computational and experimental pictures. One potentially illuminating way of building upon this experiment is to study the effects of a time-varying externally imposed shear flow on the bicoherence of turbulent fluctuations in plasma column, and to then compare those results with the results of Moyer *et al* and those presented here. Such an experiment is currently underway on the CSDX machine [41], and will be reported upon in a future publication.

These results also suggest several experimental approaches, which could allow the direct experimental study of the nonlinear dynamics of turbulence–zonal flow interactions and structure formation in confinement devices. Point-wise measurements of turbulence can be used to make qualitative comparisons of shear flow formation dynamics in experiment and simulation in a manner similar to that used in this paper. However, moving beyond such qualitative studies probably requires the application of new or emerging diagnostic and/or analysis capabilities. For example, time-resolved turbulence

775

imaging diagnostics of sufficient spatio-temporal resolution could provide evidence for the existence of streamer-like events and zonal flow structures. As shown in this paper, study of the nonlinear dynamics requires examination of the higher order statistics such as the cross-bispectrum of the potential fluctuations along with knowledge or inference of the coupling coefficients. Direct measurement of wavenumber-space resolved potential fluctuation measurements is not possible in these experiments; however, application of time-delay estimation techniques [63] to spatio-temporal density fluctuation imaging via beam-emission spectroscopy (BES) [64] may provide measurements of the fluctuating velocity field [65]. This field quantity can then, in turn, be used to find the relevant bispectrum and thus may provide a means to study nonlinear energy transfer between turbulence scales and zonal flow scales. By combining this velocity field with density fluctuations (available from BES imaging) or, in the future, with electron temperature fluctuations measured via a proposed Thomson imaging diagnostic [66], it may be possible to study turbulent particle and electron heat fluxes in the interior region of the tokamak. Such poloidally localized measurements are also needed to study the behaviour of flux PDFs, the importance of which is discussed in the following section.

5. Studies of heat flux PDFs

5.1. Theoretical summary of streamer physics, avalanches, and heat flux PDFs

Until recently, transport was modelled as a local diffusion process, described by a turbulent transport coefficient. Alas, all things must pass, and during the past 5–7 years, a growing body of experimental, theoretical, and computational evidence, which suggests that transport is bursty and intermittent has accumulated in the literature (see, e.g. Politzer [67] or Carreras *et al* [68]). Central to this idea is the notion of an 'avalanche', or 'transport event' [51]. Simply put, an avalanche is a radially extended fluctuation, extending over many correlation lengths of the elemental turbulence, which causes vigorous transport. In sandpile models, an avalanche is associated with the correlated topplings of several neighbouring cells [69, 70]. It is considerably less clear what constitutes an avalanche in a continuum model. One possibility is that an avalanche is an azimuthally symmetric 'front' or 'pulse' which flow rapidly down the gradient. Of course, such a picture presumes that the front in question is stable, i.e. that it does not undergo corrugation instability and break up into extended fingers. Another possibility is that avalanches are composed of streamers, which are radially extended, poloidally localized secondary structures [12, 13]. Such structures are equivalent to the popular notion of convective cells [71], albeit with strong poloidal localization, and with finite correlation and lifetimes. The coherent theory for nonlinear streamer formation in drift-wave turbulence is discussed in [72]. There, a set of generalized nonlinear Schrödinger equations are derived, for both streamer and zonal flow type secondary structures. The statistical, random phase approximation theory of nonlinear streamer formation in ITG turbulence is presented in [3]. Streamers are generated by modulational instability (via both vorticity and pressure advection nonlinearities), and self-regulate via the effects of their poloidally sheared radial flows, which tilt eddies and thus generate large k_θ [3], or by Kelvin–Helmholtz type instability [73]. It is interesting to note that streamer saturation levels imply that the variance of the transport flux (i.e. normalized mean square modulation) is of order unity [3], thus reinforcing the need for a statistical approach to transport.

In this paper, we focus primarily on PDF based characterizations of the heat flux. Differences between the PDFs of the local ($Q(x, y, t)$) and flux-surface averaged ($\langle Q(x, t)\rangle_y$) heat flux for the fluid models discussed in section 3 are investigated. In addition, a novel analysis technique is used to determine the PDF of 'heat pulses' (i.e. ion thermal transport avalanches) in simulations of ITG turbulence according to strength/intensity. The structure of this distribution (in particular, the power-law fit of the large pulse tail) is discussed in relation to the results of ρ^*-scaling studies of the simulation data.

5.2. Characterization of fluxes via PDFs

As described in the previous section, there is now considerable evidence that experimental turbulent transport is quite intermittent or bursty. The role of localized transport events or flux structures has also been highlighted. One method of characterizing the intermittency of a field is via the PDF of that field. Such an investigation has been carried out in the previously described (section 3) fluid models of plasma turbulence. PDFs of the local and flux-surface averaged turbulent fluxes have been calculated, the results of which are shown in figures 16 and 17, respectively. The local heat flux $Q(x, y, t)$ is defined as

$$Q(x, y, t) = pv_x = -p(x, y, t)\frac{\partial\phi(x, y, t)}{\partial y}, \qquad (14)$$

while the flux-surface averaged heat flux $\langle Q(x, t)\rangle_y$ is defined as

$$\langle Q(x, t)\rangle_y = \frac{1}{L_y}\int dy\, pv_x$$
$$= -\frac{1}{L_y}\int dy\, p(x, y, t)\frac{\partial\phi(x, y, t)}{\partial y}. \qquad (15)$$

For each case, the PDF of the quantity divided by its standard deviation is plotted; for example, figure 16(*a*) plots the PDF of $Q(x, y, t)/\overline{Q(x, y, t)}$ for the ETG case, where $\overline{Q(x, y, t)}$ is the standard deviation of $Q(x, y, t)$. Normalizing the quantities by their standard deviations allows for more accurate comparisons between the various cases.

There is a quite striking contrast between the local and averaged fluxes for both models. The local flux PDFs are strongly non-Gaussian, with extended 'wings' and high kurtosis (but little skew), while the average flux PDFs are strongly asymmetric (skewed). It should be noted that the non-Gaussian form of the local flux PDFs is not necessarily unexpected, as the flux is the product of two highly correlated variables. More significantly, it should be noted that the PDF profiles change drastically upon averaging over flux surfaces, and that there are some differences between the ITG and ETG averaged heat fluxes. Since flux-surface averaging is equivalent to removing information relating to poloidal
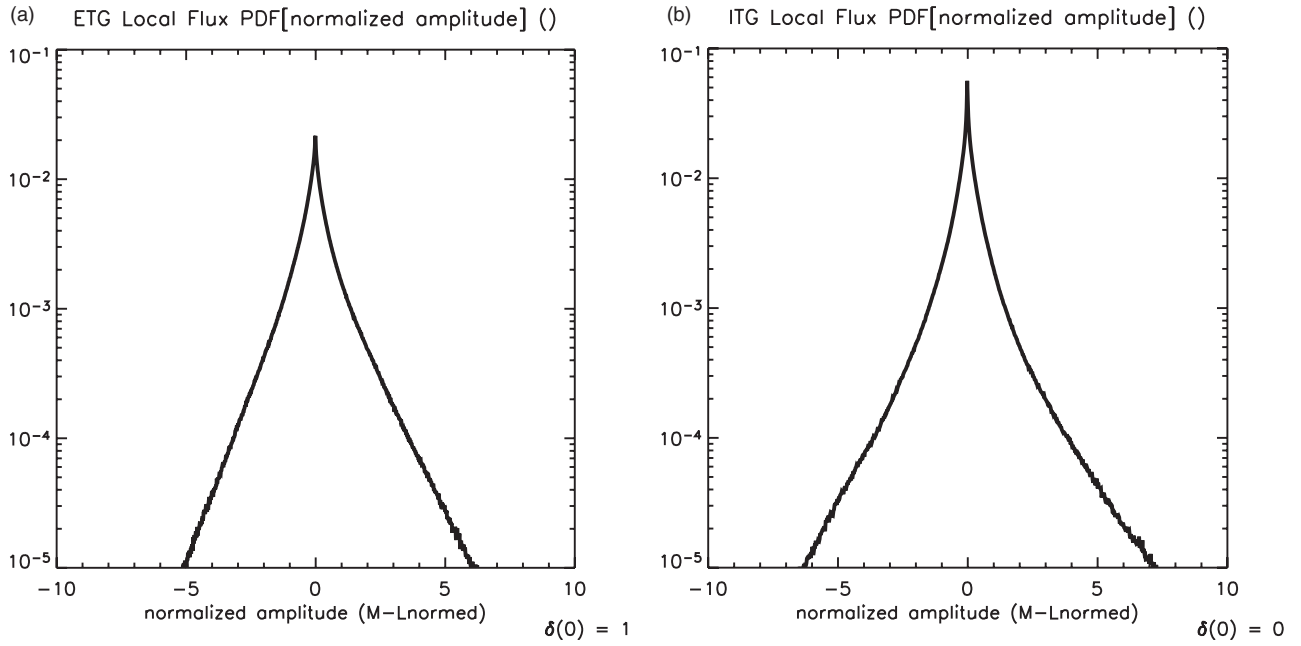
Figure 16. PDFs of local heat fluxes from ETG (*a*) and ITG (*b*) fluid models. Axes have been normalized by the PDF standard deviations.
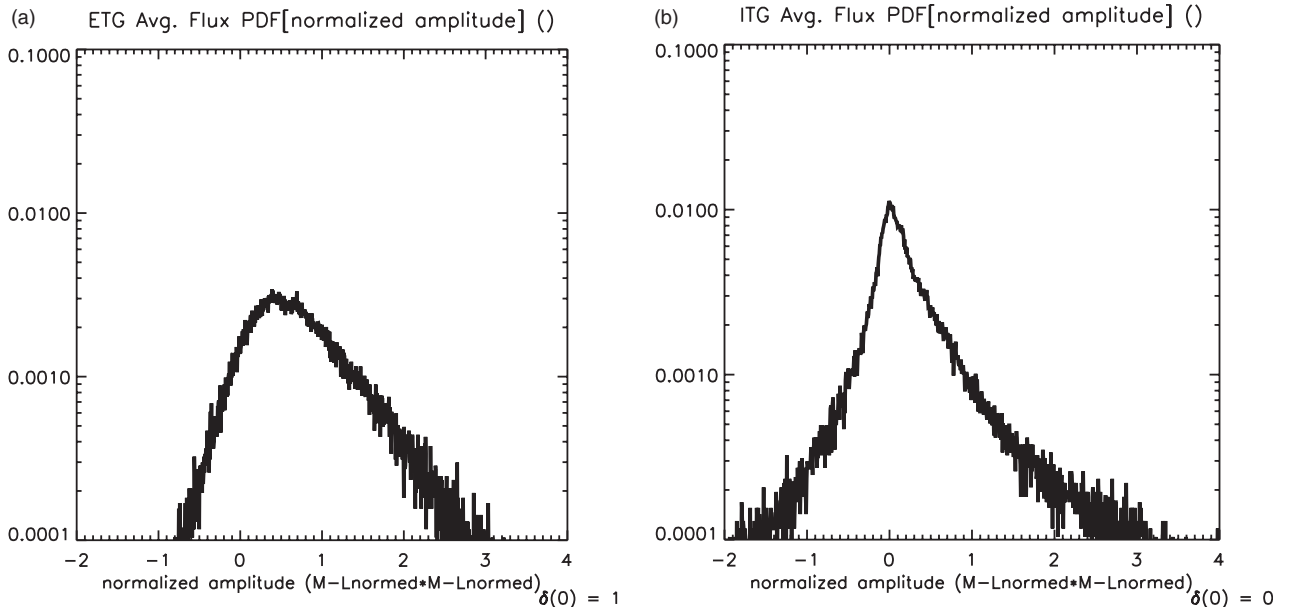
Figure 17. PDFs of flux-surfaced averaged heat fluxes from ETG (*a*) and ITG (*b*) fluid models. Axes have been normalized by the PDF standard deviations.

localization, these results suggest that poloidally localized flux structures are important components of the turbulent heat flux. Such poloidally localized, radially extended eddy structures correspond precisely to the streamers discussed previously.

5.3. Heat pulse analysis of average flux

Previous sections (5.1 and 5.2) have highlighted the importance of coherent flux structures in determining the heat flux. Extracting the true impact of these structures from single-point estimations of the flux PDF is quite difficult, as the structures will, in general, impact every moment of the PDF.

To remove this difficultly, one might note that the significant spatial resolution of simulations should allow more detailed investigations of the flux, which could incorporate the effects of correlation lengths and other intrinsic features of coherent structures.

We present here such an approach, termed 'heat pulse analysis'. In this analysis, the flux-surface averaged turbulent heat flux is decomposed into a distribution of 'pulses' of different characteristic scales; that is, $q_\perp(r, t) \equiv \sum_i q_i(r, t)$. Each $q_i(r, t)$ is positive-definite, has local support in (r, t), and has a single space/timescale. The size of the ith pulse is defined as $h_i \equiv \int \mathrm{d}r \, \mathrm{d}t \, q_i(r, t)$. The PDF of pulse sizes $f(h)$ then

777

replaces the single-point PDF of the flux. It then immediately follows that $\langle q_\perp \rangle_{r,t} = \int \mathrm{d}h\, h f(h)$. A particular advantage of this approach is that by examining how $f(h)$ falls off for large pulse-sizes, one can determine which values of h dominate the total heat flux. Examination of $f(h)$ in gyrokinetic simulations reveals that it is roughly flat for $h < h_\mathrm{c}$, and falls of as a power law $f(h) \propto h^{-\alpha}$ for $h \gg h_\mathrm{c}$. The power law dependence highlights the importance of two key scales (representing the beginning and end of the power-law tail): the small scale h_c which is set by physics, and a largest scale h_max which is set by the box size (which translates as tokamak minor radius a). If the fall-off of $f(h)$ at large h is slower than h^{-2} ($\alpha < 2$), then the heat flux is dominated by the largest heat pulses (i.e. set by h_max) and a Bohm-like scaling is obtained, while $\alpha > 2$ gives a gyroBohm-like scaling set by h_c.

To see this connection more clearly, it is useful to consider the physics behind the notions of Bohm and gyroBohm scalings. In either case, one assumes there is a turbulent diffusivity $D = (\Delta r)^2/\Delta t$, and $\Delta r/\Delta t \sim \Delta u$, so that $D \sim \Delta r \Delta u$. Estimating $\Delta u \sim V^* \sim \rho v_\mathrm{T}/a$ (assuming $a \sim L_n \sim L_\mathrm{T}$; ρ is the (thermal) gyroradius, and v_T the thermal velocity), one is left with estimating Δr. There are two natural choices for the Δr: ρ (the inherent scale of the gyromotion of the particles) or a (the largest perpendicular scale upon which fluctuations could exist). Choosing $\Delta r \sim \rho$ gives $D = D_\mathrm{GB} \sim \rho^2 v_\mathrm{T}/a$, while choosing $\Delta r \sim a$ gives $D_\mathrm{B} \sim \rho v_\mathrm{T}$. The salient point is that the global transport scaling ($D = D_\mathrm{GB}$ or $D = D_\mathrm{B}$) depends upon the characteristic scale of the transport, which may or may not depend upon the system size. What the heat pulse analysis reveals is what the characteristic scale for the heat flux is: is it the largest scale of the simulation (the $\alpha < 2$ case), or is it independent of the simulation size (the $\alpha > 2$ case). It is

in this context that we label the results as giving Bohm-like ($\alpha < 2$, transport scale set by the largest scale available to the turbulence) or gyroBohm-like ($\alpha > 2$, transport scale separate from simulation box size) scalings. Thus, while not the same as saying an actual simulation predicts a Bohm or gyroBohm transport scaling, the heat pulse analysis method does represent a clear step forward in linking the importance of large-scale, coherent flux structures predicted by theory and simulation with experimentally observed transport scalings.

An initial study using this analysis has been undertaken for results for a pair of gyrokinetic simulations of plasma turbulence (using data from the Lawrence Livermore National Laboratory code [5, 74]), with externally imposed shear flows of varying strengths; results are presented in figure 18. When the shear flow is weak or absent ('L-mode'-like, figure 18(*a*)), $\alpha = -1.524 \pm 0.1295$ (implying a Bohm-like scaling) while $\alpha = -2.279 \pm 0.1276$ (gyroBohm-like scaling) for the case of strong shear flow ('H-mode'-like, figure 18(*b*)). These results demonstrate a clear connection between the presence of large, radially extended heat flux events (manifested as $\alpha < 2$) and global scalings of transport. They also provide an intriguing counterpart to the ρ^*-scaling study of transport in a global gyrokinetic code by Lin *et al* [75]. Work is currently underway to extend the analysis to include negative values of $q_i(r, t)$ and multiple physical dimensions (in particular, to be able to more clearly capture the poloidal localization of structures such as streamers), and to apply it to the fluid models described in section 3.

6. Conclusions

In this paper, results from integrated experimental, computational, and analytic investigations of the role of nonlinear
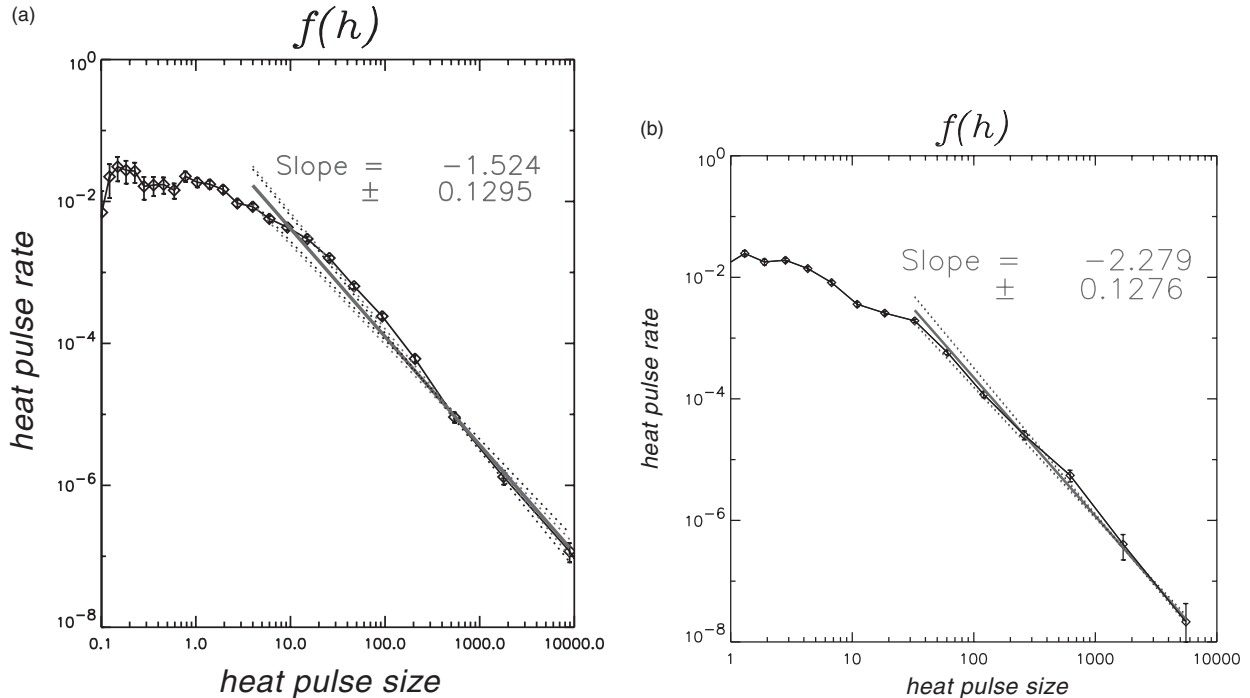
Figure 18. PDFs of heat pulse distributions for weak shear flow case (*a*) and strong shear case (*b*).

couplings in structure formation and turbulent transport regulation have been reported. The principal results are:

1. The generation of zonal flows via the turbulent Reynolds stress, and the simultaneous suppression of turbulence via 'scattering' in k_{radial} have been explicitly verified, and demonstrated to be complementary components of a single nonlinear process.

2. Significant energy transfer from zonal flows to drift-wave modes has been observed in both fluid, but not gyrokinetic simulations. A variety of nonlinear zonal flow relaxation processes are discussed, and a qualitative model for the saturated state of drift-wave turbulence, which incorporates this mechanism, is presented. In particular, the idea of zonal flow defect formation is proposed as an alternative to macro tertiary instabilities which destroy the zonal flow.

3. A simple numerical experiment which attempts to heuristically model the experimental conditions of [56] (a study of an L–H transition in DIII-D) is shown to qualitatively reproduce much of the bicoherence dynamics and structure presented in that paper, and future directions for integrated studies are motivated.

4. Significant differences in the PDFs of local and average heat fluxes for fluid models of turbulent transport have been demonstrated, highlighting the possible importance of poloidally localized structures in the flux. This result suggests that streamers and probability-based descriptions of the heat flux should be investigated more thoroughly.

5. A new method for investigating spatio-temporally resolved heat fluxes which incorporates the importance of coherent structures demonstrates a clear connection between the presence of radially extended heat flux structures predicted by theory and simulation with experimentally relevant transport scalings.

These findings motivate several future directions of inquiry. First, more comprehensive investigation of the mechanisms responsible for zonal flow saturation is needed. Examination of energy transfer in other gyrokinetic simulations for evidence of the hypothesized energy transfer 'loop' should also be undertaken (particularly as a function of deviation from marginality). Efforts to make clearer contact between experiment and simulation/theory should be continued. Finally, the heat pulse analysis technique should be refined and extended to many more sources of data, in order to build a more complete understanding of the role of coherent structures in turbulent transport.

Acknowledgments

Appendix. Ratio of zonal flow to drift-wave intensity

In a wide range of simulations of ITG turbulence, it is found that the magnitude of zonal flow intensity ($\langle|\phi_{ZF}|^2\rangle$) is almost always much greater than the peak value of the drift-wave spectrum ($\langle|\tilde{\phi}_k|^2\rangle$). This difference can easily be understood in terms of the predator–prey model of equation (1). One can recast in a zero-dimensional form [2],

$$\frac{\partial \varepsilon}{\partial t} = \gamma \varepsilon - \alpha \varepsilon U - (\Delta \omega) \varepsilon^2,$$
$$\frac{\partial U}{\partial t} = \alpha \varepsilon U - \nu_{RH} U. \tag{A1}$$

Here, ε is proportional to the total drift-wave intensity (i.e. the k-space integrated drift-wave spectrum), while γ and $\Delta\omega$ represent k-space averaged growth and nonlinear damping rates, respectively. The k_r-space diffusion term has been replaced by $-\alpha\varepsilon U$; since the scattering of drift-wave energy in k_r which the diffusion term represented is necessarily equal to the Reynolds stress drive of the zonal flow (see section 3), it then directly follows that one can replace $\gamma_{RS}U$ with $\alpha\varepsilon U$ in the zonal flow evolution equation.

It is easy to see that the model of equation (A1) has a (nontrivial) fixed point at $\varepsilon = \nu_{RH}/\alpha$, $U = (\gamma - \Delta\omega\nu_{RH}/\alpha)/\alpha$, from which it follows that the ratio of zonal flow intensity U to drift-wave intensity ε is

$$\frac{U}{\varepsilon} = \frac{\gamma}{\nu_{RH}} - \frac{\Delta\omega}{\alpha}. \tag{A2}$$

For realistic parameters, $\gamma/\nu_{RH} \gg 1$, $\Delta\omega/\alpha$ ($\Delta\omega/\alpha \sim O(1)$ in normalized units). Therefore, the fact that zonal flow intensity is found to be larger than the drift-wave intensity is a natural consequence of the ratio of linear drift-wave growth rate to zonal flow damping rate being much larger than one.

References

[1] Hasegawa A. and Wakatani M. 1987 *Phys. Rev. Lett.* **59** 431
[2] Diamond P.H. *et al* 1998 *Proc. 17th IAEA Fusion Energy Conf. (Yokohama, Japan, 1998, 1999), Proc. 17th Int. Conf. on Fusion Energy 1998 (Yokohama, 1998)* (Vienna: IAEA) CD-ROM file TH3/1, http://www.iaea.org/programmes/ripc/physics/start.htm
[3] Diamond P.H. *et al* 2001 *Nucl. Fusion* **41** 1067
[4] Hammett G.W. *et al* 1993 *Plasma Phys. Control. Fusion* **35** 973
[5] Dimits A.M., Williams T.J., Byers J.A. and Cohen B.I. 1996 *Phys. Rev. Lett.* **77** 71
[6] Sydora R.D. *et al* 1996 *Plasma Phys. Control. Fusion* **38** A281
[7] Lin Z. *et al* 1998 *Science* **281** 1835
[8] Lin Z. *et al* 1999 *Phys. Rev. Lett.* **83** 3645
[9] Diamond P.H. and Kim Y.-B. 1991 *Phys. Fluids* **3** 1626
[10] Biglari H., Diamond P.H. and Terry P.W. 1990 *Phys. Fluids* B **2** 1
[11] Hahm T.S. and Burrell K.H. 1995 *Phys. Plasmas* **2** 1648
[12] Drake J.F., Guzdar P.N. and Hassam A.B. 1988 *Phys. Rev. Lett.* **61** 2205
[13] Beyer P., Benkadda S., Garbet X. and Diamond P.H. 2001 *Phys. Rev. Lett.* **87** 015001
[14] Chen L., Lin Z. and White R. 2000 *Phys. Plasmas* **7** 3129
[15] Horton W. 1999 *Rev. Mod. Phys.* **71** 735
[16] Frisch U. 1995 *Turbulence* (Cambridge: Cambridge University Press)
[17] Kraichnan R.H. 1967 *Phys. Fluids* **10** 1417

[18] Rosenbluth M.N. and Hinton F.L. 1998 *Phys. Rev. Lett.* **80** 724
[19] Rogers B., Dorland W. and Kotschenreuther M. 2000 *Phys. Rev. Lett.* **85** 5336
[20] Malkov M, Diamond P.H. and Smolyakov A.I. 2001 *Phys. Plasmas* **8** 1553
[21] Marchenko V.S. 2002 *Phys. Rev. Lett.* **89** 185002
[22] Kaw P., Singh R. and Diamond P.H. 2002 *Plasma. Phys. Control. Fusion* **44** 51
[23] Smolyakov A.I, Diamond P.H. and Malkov M. 2000 *Phys. Rev. Lett.* **84** 491
[24] Diamond P.H. *et al* 2000 *Phys. Rev. Lett.* **84** 4842
[25] Smolyakov A.I. and Diamond P.H. 1999 *Phys. Plasmas* **6** 4410
[26] Waltz R.E., Kerbel G.D., Milovich J. and Hammett G.W. 1994 *Phys. Plasmas* **1** 2229
[27] Waltz R.E., Kerbel G.D., Milovich J. and Hammett G.W. 1995 *Phys. Plasmas* **2** 2408
[28] Horton W., Choi D.I. and Tang W.M. 1981 *Phys. Fluids* **24** 1077
[29] Horton W., Hong B.G. and Tang W.M. 1988 *Phys. Fluids* **31** 2971
[30] Jenko F., Dorland W., Kotschenreuther M. and Rogers B.N. 2000 *Phys. Plasmas* **7** 1904
[31] Holland C. and Diamond P.H. 2002 *Phys. Plasmas* **9** 3857
[32] Jenko F. and Kendl A. 2002 *New J. Phys.* **4** 35
[33] Kim E., Holland C. and Diamond P.H. Collisional damping of ETG mode driven zonal flows *Phys. Plasmas* submitted
[34] Idomura Y., Wakatani M. and Tokuda S. 2000 *Phys. Plasmas* **7** 3551
[35] Frieman E.A. and Chen L. 1982 *Phys. Fluids* **25** 502
[36] Lee W.W. 1983 *Phys. Fluids* **26** 556
[37] Bewley T.R. 1999 Optimal and robust control and estimation of transition, convection, and turbulence *PhD Thesis* Stanford University
[38] Carmargo S.J., Biskamp D. and Scott B.D. 1995 *Phys. Plasmas* **2** 48
[39] Hasegawa A. and Wakatani M. 1983 *Phys. Rev. Lett.* **50** 682
[40] Gang F.Y., Diamond P.H., Crotinger J.A. and Koniges A.E. 1991 *Phys. Fluids* B **4** 955
[41] George J. 2001 Experimental study of linear resistive drift waves in a quiescent cylindrical plasma *MS Thesis* University of California, San Diego
[42] Burin M., Antar G., Crocker N. and Tynan G.R. Development of collisional drift wave turbulence in a helicon plasma device *Phys. Plasmas* submitted
[43] Candy J. and Waltz R.E. 2003 *J. Comput. Phys.* **186** 545
[44] Dimits A. *et al* 2000 *Phys. Plasmas* **7** 969
[45] Watanabe S. and Sugama H. 2002 *Phys. Plasmas* **9** 3659
[46] Kim E. and Diamond P.H. 2002 *Phys. Plasmas* **9** 4530
[47] Hinton F.L. and Rosenbluth M.N. 1999 *Plasma Phys. Control. Fusion* **41** A653
[48] Scott B.D., Terry P.W. and Diamond P.H. 1988 *Phys. Fluids* **31** 1481
[49] Rosenbluth M.N. 2001 University of California, San Diego, Hinton F.L., General Atomics, Private communication
[50] Gill A.E. 1965 *J. Fluid. Mech.* **21** 503
[51] Diamond P.H. and Hahm T.S. 1995 *Phys. Plasmas* **2** 3640
[52] Hwa T. and Kardar M. 1992 *Phys. Rev.* A **45** 7002
[53] Kim Y.C. and Powers E.J. 1978 *Phys. Fluids* **21** 1452
[54] Kim Y.C. and Powers E.J. 1979 *IEEE Trans. Plasmas Sci.* **2** 120
[55] Ritz Ch.P., Powers E.J. and Bengtson R.D. 1989 *Phys. Fluids* B **1** 153
[56] Moyer R.A., Tynan G.R., Holland C. and Burin M.J. 2001 *Phys. Rev. Lett.* **87** 135001
[57] Tynan G.R., Moyer R.A., Burin M.J. and Holland C. 2001 *Phys. Plasmas* **8** 2691
[58] Holland C. *et al* 2002 *Plasma Phys. Control. Fusion* **44** A453
[59] Kim E. and Diamond P.H. 2003 *Phys. Plasmas* **10** 1698
[60] Kim E. and Diamond P.H. 2003 *Phys. Rev. Lett.* **90** 185006
[61] Winsor N., Johnson J.L. and Dawson J.M. 1968 *Phys. Fluids* **11** 2448
[62] Hallatschek K. and Biskamp D. 2001 *Phys. Rev. Lett.* **86** 1223
[63] Jakubowski M., Fonck R.J., Fenzi C. and McKee G.R. 2001 *Rev. Sci. Instrum.* **72** 996
[64] McKee G.R., Fenzi C. and Fonck R.J. 2002 *IEEE Trans. Plasma Sci.* **30** 62
[65] Jakubowski M., Fonck R.J. and McKee G.R. 2002 *Phys. Rev. Lett.* **88** 265003
[66] Zweben S.J. *et al* 2001 *Rev. Sci. Instrum.* **72** 1
[67] Politzer P.A. 2000 *Phys. Rev. Lett.* **84** 1192
[68] Carreras B.A. *et al* 2000 *Phys. Plasmas* **7** 3278
[69] Bak P., Tang C. and Wisenfeld K. 1987 *Phys. Rev. Lett.* **59** 381
[70] Jensen H.J. 1998 *Self-Organized Criticality* (Cambridge: Cambridge University Press)
[71] Sagdeev R.Z., Shapiro V.D. and Shevchenko V.I. 1978 *Sov. J. Plasma Phys.* **4** 306
[72] Champeaux S. and Diamond P.H. 2001 *Phys. Lett.* A **288** 214
[73] Cowley S.C., Kulsrud R.M. and Sudan R. 1991 *Phys. Fluids* B **3** 2767
[74] Dimits A.M. *et al* 2000 *Nucl. Fusion* **40** 661
[75] Lin Z., Either S., Hahm T.S. and Tang W.M. 2002 *Phys. Rev. Lett.* **88** 195004